

# FORMSpOT: A Decade of Tree-Level, Country-Scale Forest Monitoring

Martin Schwartz<sup>a</sup>, Fajwel Fogel<sup>b</sup>, Nikola Basic<sup>c,d</sup>, Damien Robert<sup>e</sup>, Louis Geist<sup>f</sup>, Jean-Pierre Renaud<sup>c,d,g</sup>, Jean-Matthieu Monnet<sup>h</sup>, Clemens Mosig<sup>i</sup>, Cédric Vega<sup>c,d</sup>, Alexandre d’Aspremont<sup>b</sup>, Loïc Landrieu<sup>f</sup>, Philippe Ciaia<sup>a</sup>

<sup>a</sup>Laboratoire des Sciences du Climat et de l’Environnement (LSCE), CEA, CNRS, UVSQ, Université Paris-Saclay, Gif-sur-Yvette, France

<sup>b</sup>CNRS & Département d’Informatique, École Normale Supérieure – PSL, 45 Rue d’Ulm, 75005, Paris, France

<sup>c</sup>Université Gustave Eiffel, Géodata Paris, IGN, LIF, Nancy, 54000, France

<sup>d</sup>Université de Lorraine, Géodata Paris, IGN, LIF, Nancy, 54000, France

<sup>e</sup>EcoVision Lab, DM3L, University of Zurich, Switzerland

<sup>f</sup>LIGM, École des Ponts, CNRS, IPP, UGE,

<sup>g</sup>Office National des Forêts, Pôle Recherche et Développement Innovation, 8 Allée de Longchamp, Villier-les-Nancy, 54600, France

<sup>h</sup>Université Grenoble Alpes, INRAE, LESSEM, 2 rue de la Papeterie-BP 76, 38402, St-Martin-d’Hères, France

<sup>i</sup>Institute of Earth System Science and Remote Sensing, Leipzig, Germany

---

## Abstract

The recent decline of the European forest carbon sink highlights the need for spatially explicit and frequently updated forest monitoring tools. Yet, existing satellite-based disturbance products remain too coarse to detect changes at the scale of individual trees, typically below 100 m<sup>2</sup>. Here, we introduce **FORMSpOT** (Forest Mapping with SPOT Time series), a decade-long (2014–2024) nationwide mapping of forest canopy height at 1.5 m resolution, together with annual disturbance polygons (**FORMSpOT-Δ**) covering mainland France. Canopy heights were derived from annual SPOT-6/7 composites using a hierarchical transformer model (PVTv2) trained on high-resolution airborne laser scanning (ALS) data. To enable robust change detection across heterogeneous acquisitions, we developed a dedicated post-processing pipeline combining co-registration and spatio-temporal total variation denoising. Validation against ALS revisits across 19 sites and 5,087 National Forest Inventory plots shows that FORMSpOT-Δ substantially outperforms existing disturbance products. In mountainous forests, where disturbances are small and spatially fragmented, FORMSpOT-Δ achieves an F1-score of 0.44, representing an order of magnitude higher than existing benchmarks. By enabling tree-level monitoring of forest dynamics at national scale, FORMSpOT-Δ provides a unique tool to analyze management practices, detect early signals of forest decline, and better quantify carbon losses from subtle disturbances such as thinning or selective logging. These results underscore the critical importance of sustaining very high-resolution satellite missions like SPOT and open-data initiatives such as DINAMIS for monitoring forests under climate change.

**Keywords:** Deep Learning, Forest height, Time Series, SPOT, ALS, Vision Transformers, Forest disturbances

---

## 1. Introduction

Global forests absorb 3.5 PgC yearly, which represents almost half of anthropogenic fossil fuel emissions, but almost two-thirds of this newly sequestered carbon is annulled by tropical deforestation (Pan et al., 2024). Monitoring forest evolution is therefore essential to follow above-ground carbon dynamics and adopt sustainable management practices. While the dominant driver of forest carbon loss in tropical ecosystems is deforestation, harvest and natural mortality are the main drivers of European carbon losses, representing 85% and 15% of forest disturbances in Europe, respectively (Ritter et al., 2025). The European Union (EU) strongly relies on

forests to fulfill its international engagement in the Paris Agreement with the European Green Deal that aims for carbon neutrality by 2050 (EU, 2024). However, this commitment is compromised by the recent drop in the EU’s forest sink (Korosuo et al., 2023) due to a decline in forest productivity (Ols et al., 2020; Hertzog et al., 2025) and tree mortality rate doubling since 1984 (Senf et al., 2018; IGN, 2025c). Accurately monitoring EU’s forests is thus needed to achieve such climate goals. National forest inventories (NFIs) play a key role in monitoring forests (Cateau et al., 2024; Breidenbach et al., 2021; Shvidenko and Nilsson, 2002). In France, for example, the French NFI carries out yearly field data collection campaigns, focusing on tree height, diameter, and

species, on over 5,000 new plots each year. Additionally, since 2010, revisits started on plots sampled five years earlier. Although each plot is measured only twice (semi-permanent design), these rolling revisits allow annual estimates of forest fluxes from growth, mortality and recruitment (Bontemps and Bouriaud, 2024). However, NFIs do not enable spatially continuous monitoring of forests and are constrained by their reporting based on observations spanning across multiple years. Remote sensing (RS) technologies can complement these inventory measurements (Tomppo et al., 2008; Nilsson et al., 2017; Saarela et al., 2020; Network, 2025) and obtain more frequent and spatially continuous maps of forest attributes. In particular, airborne laser scanning (ALS) technologies are widely regarded as the gold standard for obtaining detailed 3D structural information about forest canopies (Vepakomma et al., 2008). In France, the Lidar HD initiative (IGN, 2025a) aims to cover the entire country with high-density ( $>10$  points/m<sup>2</sup>) ALS acquisitions, providing a country-wide snapshot of the French forests. However, given that data renewal is not guaranteed and may vary in space and time, ALS cannot be regarded as a dependable source of information on temporal dynamics. In most cases, LiDAR campaigns are conducted on decadal timescales, which are insufficient for addressing the rapid changes brought about by climate change and anthropogenic activities (Shi et al., 2025; Risbøl et al., 2020).

Satellite-based remote sensing has become an important complement to traditional forest monitoring methods. Satellite imagery provides far wider and cheaper spatial coverage than ALS, but often lacks the detailed 3D structural information that ALS offers. Recent work in geospatial machine learning shows that deep models can learn mappings from multispectral optical imagery to per-pixel canopy height, effectively approximating LiDAR-derived structural metrics at large scale. A wide range of forest-related applications has derived from these new approaches such as monitoring African forests carbon dynamics (Bossy et al., 2025), monitoring forest height and biomass at the country level (Schwartz et al., 2023; Su et al., 2025; Lang et al., 2019), complementing NFI data that cannot be collected during war time in Ukraine (Lukeš et al., 2025; Myroniuk et al., 2024), following carbon stocks in agroforestry plantations (D'Amico et al., 2025), or estimating post-fire biomass losses (Vallet et al., 2023; Pontes-Lopes et al., 2022).

Several approaches have already been used to monitor forest disturbances from satellite RS data: Near-real-time forest disturbance alerts, mostly for tropical regions, generally rely on synthetic aperture radar (SAR)

imagery from Sentinel-1 to overcome cloud coverage issues (Reiche et al., 2021; Bouvet et al., 2018; Ballère et al., 2021; Ygorra et al., 2021; Mullissa et al., 2024). These systems support local actions and help protect forest ecosystems from illegal activities (Moffette et al., 2021). Comparable products also exist in temperate regions. For example, the SUFOSAT project (Mermoz et al., 2024) provides sub-monthly monitoring of clearcuts across mainland France using Sentinel-1 time-series analysis. Similarly, for longer-term monitoring, where near-real-time updates are not required, optical imagery is commonly used to characterize forest disturbances. The European Forest Disturbance Atlas (Viana-Soto and Senf, 2025), for example, uses the Landsat archive to map and attribute disturbance events across European forests since 1985 using a random forest-based classification approach. Similarly, Turubanova et al. (2023) derived an annual tree canopy removal product across Europe from Landsat data starting in 2000 based on forest height. At the global scale, the forest cover change product from Hansen et al. (2013) also relies on Landsat imagery to enable consistent disturbance monitoring worldwide.

However, the spatial resolution of these products (10 m for S1 and 30 m for Landsat) is too coarse to detect small disturbances below 100 m<sup>2</sup> reliably and thus cannot detect selective logging events, isolated tree mortality, and gap formation due to pest attacks (Krüger et al., 2024). These small disturbances can represent a significant fraction of forest carbon losses. Espírito-Santo et al. (2014) showed, for instance, that the small losses ( $< 0.1$  ha) in Amazonian forests account for 98% of forest carbon losses in this region. Mapping the spatio-temporal pattern of mortality is also key to understanding the effects of climate change and management on forest dynamics. In the past decade, developments in remote sensing and satellite technology have enabled the acquisition of very high-resolution (VHR) imagery ( $< 2$  m resolution), approaching the quality of airborne data. For example, the WorldView-110 camera onboard the WorldView-3 satellite (Maxar Technologies, launched in 2014) and the radiometer onboard the Pleiades satellites (developed by the French Space Agency, CNES) both provide spaceborne imagery with spatial resolutions below 50 cm. In France, the DataTerra Dinamis Open Data initiative<sup>1</sup> makes optical SPOT-6/7 imagery from the SPOT-6/7 constellation (Airbus Defence and Space) freely available, providing RGB yearly country-wide mosaics at 6 m resolution and

---

<sup>1</sup><https://openspot-dinamis.data-terra.org/>

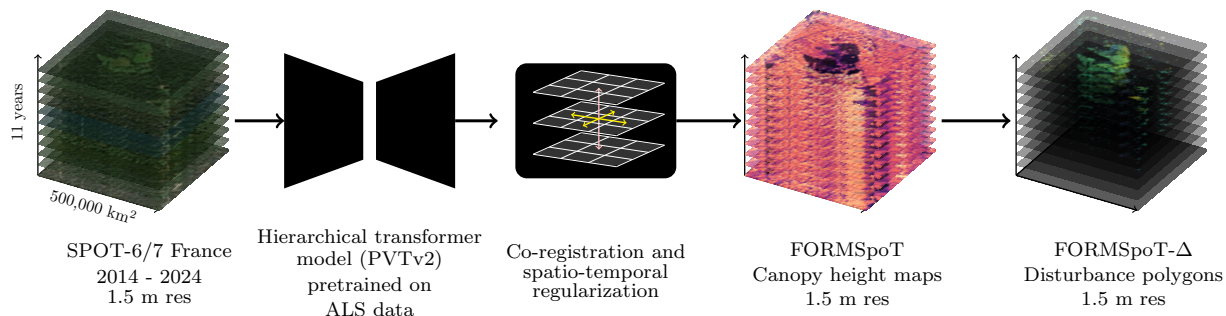


**Figure 1: Overview of the workflow used to generate FORMSpOT and FORMSpOT- $\Delta$ .** SPOT-6/7 images over mainland France at 1.5 m resolution (2014–2024) were processed with a pretrained PVTv2 model (Fogel et al., 2025) to produce annual forest canopy height maps. These height maps were then co-registered and spatio-temporally regularized to ensure consistency across the time series. From the resulting 1.5 m annual canopy height time series (FORMSpOT), disturbance polygons (FORMSpOT- $\Delta$ ) were extracted by applying a 5 m height-loss threshold and a morphological filter.

panchromatic images at 1.5 m resolution since 2014. SPOT data has been used for various forestry applications (Ali et al., 2024; Rahimizadeh et al., 2019; Li et al., 2015). Until now, however, its use for retrieving canopy height and identifying forest disturbances had only been demonstrated at limited spatial and temporal scales (Fogel et al., 2025). Recent progress in deep learning (DL) has made it possible to use VHR data for multiple applications in forestry, especially when coupled with dense LiDAR datasets. For example, Tucker et al. (2023) used Maxar imagery alongside convolutional neural networks to map individual trees and derive tree heights from their shadows in African drylands. This approach complements carbon estimations in this region by including the biomass from trees that were overlooked in coarser resolution biomass estimations. On a global scale, Tolan et al. (2023) used a transformer-based model (DINOv2) trained on ALS acquisitions to map tree heights globally at 1 m from Maxar imagery. At the European level, Liu et al. (2023) leveraged PlanetScope data to build the first European forest height map at 3 m resolution from a U-Net model trained on ALS acquisitions. Some studies have also used VHR coupled with a DL algorithm to detect tree removals, such as Brandt et al. (2024), who mapped the degradation of farmland trees in India due to changes in agricultural practices, and Cheng et al. (2024), who evaluated scattered tree death in California.

However, to date, no study has used a long-term time series of VHR imagery to allow for mapping of yearly tree-level disturbances across an entire country. Here, we present annual forest canopy height (FORMSpOT) and disturbance (FORMSpOT- $\Delta$ ) products covering metropolitan France (551,695 km<sup>2</sup>, the largest country in the European Union) over a period of eleven years (2014–2024). Using a hierarchical trans-

former model (PVTv2) trained on dense aerial lidar scans, we predict annual canopy heights from SPOT-6/7 imagery with a spatial resolution of 1.5 metres. To ensure temporal and spatial consistency between yearly predictions, we first apply a spatial registration procedure and then a variational smoothing approach to mitigate noise and enhance the robustness of our predictions over time. The resulting spatio-temporal data cube of annual canopy height maps (FORMSpOT) provides a unique perspective on the evolution of French forests over the past decade and enables the detection of subtle forest disturbances (FORMSpOT- $\Delta$ ) that would be impossible to observe at coarser resolutions. Through extensive in situ validation using ground measurements and repeated LiDAR campaigns, we demonstrate the accuracy and reliability of our maps. Our emphasis on high-resolution monitoring demonstrates that scalable, data-driven methods are critical to dynamic forest management in a context of climate change.

## 2. Data and methods

### 2.1. Data

This study relies on a model trained using high-resolution airborne laser scanning (ALS) data from the French LiDAR HD program as reference height measurements (Section 2.1.1), and on SPOT-6/7 satellite imagery (Section 2.1.2) used as predictors to derive annual canopy height maps. We further validated our FORMSpOT- $\Delta$  disturbance polygons using successive ALS acquisitions from LiDAR HD and additional sources (Section 2.1.3). Complementary validation of both FORMSpOT and FORMSpOT- $\Delta$  was performed using repeated measurements from the French National

Forest Inventory (NFI; Section 2.1.4). All validations included a comparison with existing disturbance products available over France (Section 2.1.5).

### 2.1.1. LiDAR HD ALS

The French LiDAR HD program, coordinated by the National Institute of Geographic and Forest Information (IGN), is a nationwide Airborne Laser Scanning (ALS) survey. Launched in 2021, this mission acquires high-resolution point clouds ( $>10$  pts/m<sup>2</sup>) to produce a single snapshot of the 3D structure of the French mainland territory. In this study, LiDAR HD data were used in two distinct ways. First, ALS-derived canopy height models (CHMs) served as a reference to train a deep neural network that maps SPOT-6/7 imagery to dense estimates of canopy height. These reference CHMs were obtained from Open-Canopy (Fogel et al., 2025), a public benchmark dataset for high-resolution canopy height estimation. Second, LiDAR HD data were used to validate the FORMSpOT- $\Delta$  disturbance polygons. In this case, we directly used the canopy height models (CHMs) processed by IGN at a 0.5 m resolution (IGN, 2025a). By comparing CHMs acquired at different dates from Lidar HD and other sources (See Section 2.1.3), we identified canopy-height changes and delineated disturbance polygons to validate FORMSpOT- $\Delta$  (See Section 2.2.4).

### 2.1.2. SPOT-6/7 data

The SPOT Earth observation program was initiated in the 1970s by the French Space Agency (CNES) to support a broad range of remote sensing applications. The SPOT-6/7 constellation consisted of two satellites launched in 2012 and 2014, which acquire optical imagery in four spectral bands (R: red, G: green, B: blue, and NIR: near-infrared) at 6 m resolution, along with a 1.5 m panchromatic band. SPOT 7 was decommissioned in March 2023 due to an orbit failure. Country-wide, orthorectified SPOT-6/7 mosaics over France (2014–2024) are freely distributed annually through the DINAMIS platform<sup>2</sup> under the open Etalab-2 license. To produce these mosaics, metropolitan France is divided into 240 overlapping acquisition tiles that guide the yearly programming of the SPOT-6/7 constellation. Each year, between 400 and 600 images are collected over these tiles, and the 240 best are selected to assemble the annual, almost cloud-free, coverage of the French territory (DINAMIS, 2020). For this study, we retrieved the multispectral (6 m) and panchromatic (1.5 m) versions of these images and applied a pansharpening pro-

cedure implemented in GDAL (GDAL/OGR contributors, 2025) to produce multispectral data at 1.5 m resolution. In the following, we refer to each pansharpened image simply as a “SPOT-6/7 image.” The resulting dataset corresponds to 800 GB per year after pansharpening and compression using the Zstandard algorithm (Collet and Kucherawy, 2021). We first trained our model on a subset of the SPOT-6/7 data (See Section 2.2.1) and then used the entire dataset to derive yearly height maps at a 1.5 m resolution.

### 2.1.3. Successive ALS acquisitions

To validate FORMSpOT- $\Delta$  polygons, we used reference polygons derived from successive ALS acquisitions at 19 sites distributed across France (Fig. 2).

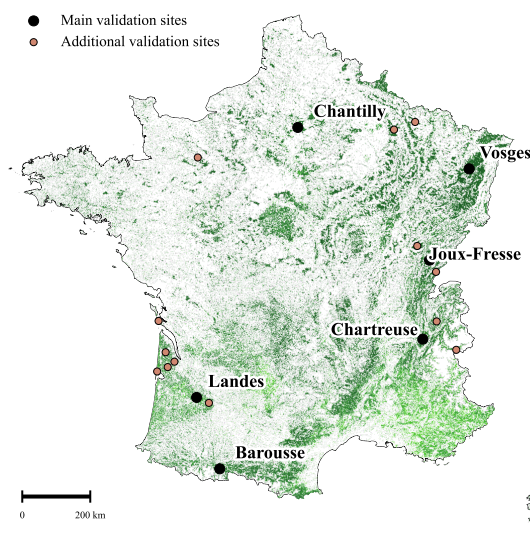


**Figure 2: FORMSpOT- $\Delta$  validation sites.** Locations of the 19 ALS sites used to validate FORMSpOT- $\Delta$  polygons. The six sites presented in the main part of this study are highlighted in bold black font. Additional validation sites, whose metrics are presented in the supplementary materials (Fig. S2), are indicated with smaller orange dots. Greenness represents tree cover density (CLMS, 2023).

All acquisitions have a high point density ( $>5$  pts/m<sup>2</sup>) and were processed to obtain CHMs at 1 m resolution. In this study, we selected six main validation sites to cover a broad range of forest and terrain configurations (Table 1). These include high mountainous regions, where detecting disturbances is particularly challenging (e.g., Chartreuse, Barousse); lower mountains with mixed forests (e.g., Vosges, Joux-Fresse); and low-relief areas such as an intensively managed maritime pine plantation (Landes) and a declining oak forest (Chantilly). In Chantilly, salvage logging of declining oaks creates sparse, tree-level canopy openings, representing

<sup>2</sup><https://openspot-dinamis.data-terra.org/>

**Table 1: Description of the 6 main ALS sites used to validate FORMSpOT- $\Delta$  polygons.** Site locations are presented in Fig. 2. All ALS point clouds ( $>5$  pts/m<sup>2</sup>) were processed to obtain 1 m resolution CHMs. The description and results for other validation sites can be found in the supplementary materials.

Site name	Forest type	Date and source 1	Date and source 2	Area
Landes 	Maritime pine plantations around the Ciron river	Oct. 2019 – FRISBEE research project (Durrieu et al., 2025b)	March 2021 – FRISBEE research project (Durrieu et al., 2025a)	~1,500 ha
Chantilly 	Declining deciduous oak forest with salvage logging over a flat area (Le Boulter, 2023)	Feb. 2022 – Lidar HD, IGN	Sep. 2023 – Requested to Laurent Saint-André and the collective “Ensemble Sauvons la forêt de Chantilly.”	~7,000 ha
Joux-Fresse 	Coniferous in low mountains (Jura)	June 2019 – Office National des Forêts (ONF)	Aug. 2022 – Lidar HD, IGN	~6,000 ha
Vosges 	Mixed forests (beech, fir, spruce) in low mountainous areas (Vosges)	Feb. 2020 – IGN, see (Ramirez Parra et al., 2024) for description	Apr. 2022 – Lidar HD, IGN	~225,000 ha
Chartreuse 	Mixed forest, in high mountainous areas (Alps)	Sep. 2016 – Office National des Forêts (ONF)	Sep. 2021 – Lidar HD, IGN	~9,000 ha
Barousse 	Mixed forest, in high mountainous areas (Pyrenees)	Sep. 2019 – Office National des Forêts (ONF)	Sep. 2021 – Lidar HD, IGN	~5,200 ha

small-scale disturbances. The detailed point density of each ALS acquisition, along with the analysis relative to the other sites, is presented in the supplementary materials attached to this paper.

#### 2.1.4. French NFI

The French National Forest Inventory (NFI) collects measurements from over 10,000 field plots annually across the country. Within each 30 m diameter plot, dendrometric attributes (e.g., tree height, diameter) and various environmental indicators (e.g., tree health, soil characteristics) are recorded. To validate our FORMSpOT height estimates (See Section 2.2.3), we compared the height of the tallest tree measured in each NFI plot with the maximum FORMSpOT pixel value within an 18 m radius around the plot center. This radius corresponds to the plot extent plus an additional 3 m buffer to account for potential geolocation uncertainty of NFI’s plot geolocation. Plots located within areas used for model training were excluded from this validation.

Since 2010, all plots have been re-measured on a five-year cycle, providing repeated observations of tree diameter and indicators of forest health. We used the NFI plot revisits to compute the percentage of trees that disappeared within the 2018–2023 five-year interval and compared these values with our predicted disturbance polygons (FORMSpOT- $\Delta$ , see Section 2.2.4). The French

NFI can be accessed online<sup>3</sup>, however, exact plot locations are subject to statistical confidentiality and can only be used for research product validation purposes through anonymous data matching.

#### 2.1.5. Other studies used for comparison

To assess the performance of the FORMSpOT- $\Delta$  disturbance polygons relative to existing country-wide products for France, we compared our results with several previously published datasets (Table 2). Some of these rely on Landsat imagery at 30 m resolution: Hansen et al. (2013), Turubanova et al. (2023), and the European Forest Disturbance Atlas (EFDA; Viana-Soto and Senf (2025)). Others are derived from Sentinel-1 and/or Sentinel-2 data: SUFOSAT (Mermoz et al., 2024), FORMS-T (Schwartz et al., 2025), Pauls et al. (2025), and deadtrees.earth (Mosig., 2026; Mosig et al., 2026). The latter three datasets do not explicitly provide disturbance polygons. We therefore extracted them by applying a 5 m height-loss threshold to their best height products (FORMS-T and Pauls) to be consistent with the threshold applied to FORMSpOT to derive FORMSpOT- $\Delta$  polygons (See Section 2.2.4). For deadtrees.earth, which is a fractional tree cover product, we used a 25% forest cover loss threshold, corresponding to

<sup>3</sup><https://inventaire-forestier.ign.fr/dataifn/?lang=en>

**Table 2: Forest disturbance detection products.** Note that available years for height products correspond to the years for which we can obtain loss polygons. For instance, FORMS-T spans the 2018-2024 period but forest loss polygons can only be calculated for the years 2019-2024. The deadtrees.earth model works at global coverage, and data from the sites introduced in Section 2.1.3 were produced for this study (<https://deadtrees.earth/deadtrees>).

Name	Source	Type	Methods	Years	Res.	Data used	Extent
FORMSpOT- $\Delta$	This study	Disturbance polygons derived from forest height (5 m loss threshold)	PVTv2 hierarchical Vision Transformer trained on SPOT-6/7 and ALS heights	2015 2024	1.5 m	SPOT-6/7	France
Pauls	Pauls et al. (2025)	Disturbance polygons derived from forest height (5 m loss threshold)	3D U-Net trained on S1 and S2 imagery with GEDI heights as reference label	2020 2022	10 m	Sentinel-1, Sentinel-2	Europe
FORMS-T	Schwartz et al. (2025)	Disturbance polygons derived from forest height (5 m loss threshold)	U-Net convolutional neural network trained on S1, S2 and GEDI heights	2019 2024	10 m	Sentinel-1, Sentinel-2	France
deadtrees.earth	Mosig et al. (2026); Mosig. (2026)	Disturbance polygons derived from fractional forest cover change (25% loss threshold)	Fractional forest cover upscaled from drone to Sentinel-2 pixel timeseries with transformer.	2018 2025	10 m	Sentinel-2	Global
Hansen	Hansen et al. (2013)	Tree cover loss product	Bagged decision trees with Landsat	2000 2024	30 m	Landsat	Global
Turubanova	Turubanova et al. (2023)	Tree removal product derived from tree height maps	Bagged regression tree on Landsat	2002 2021	30 m	Landsat	Europe
SUFOSAT	Mermoz et al. (2024)	Forest clearcuts	Algorithm based on Sentinel-1 shadowing effect	2017 2025	10 m	Sentinel-1	France
EFDA	Viana-Soto and Senf (2025)	Forest disturbances	Random Forest with Landsat	1985 2023	30 m	Landsat	Europe

the value giving the best F1 score across all sites for this dataset (See Section 2.2.5).

## 2.2. Methods

To generate a consistent forest height time series (FORMSpOT) and derive disturbance polygons (FORMSpOT- $\Delta$ ), we applied a multi-step processing pipeline. First, a pretrained vision transformer model (Fogel et al., 2025) was used to produce initial height predictions from the SPOT-6/7 imagery (Section 2.2.1). These predictions were then averaged over overlapping images and temporally co-registered (Section 2.2.2). A denoising procedure was applied to obtain a temporally consistent height series, hereafter referred to as FORMSpOT (Section 2.2.3). Finally, year-to-year differences of these height maps were used to derive disturbance polygons, referred to as FORMSpOT- $\Delta$  (Section 2.2.4). We further validated FORMSpOT- $\Delta$  with metrics relying on ALS-derived disturbance polygons, and successive NFI measurements (Section 2.2.5). The full methodology is described in the following sections.

### 2.2.1. Height estimations

In this study, we used the hierarchical transformer model PVTv2 (Wang et al., 2022), pretrained on the Open-Canopy dataset (Fogel et al., 2025), which contains over 100,000 km<sup>2</sup> of co-registered SPOT-6/7 images and ALS-derived canopy height maps. We applied this model to the SPOT-6/7 images covering France for 2014-2024 (Section 2.1.2) to obtain the initial height predictions. Formally, we considered a temporal stack of SPOT-6/7 images  $x \in \mathbf{R}^{T \times C \times H \times W}$ , where  $T$  is the number of scanned years (here  $T = 11$ ),  $C$  the number of channels (here  $C = 4$ , corresponding to RGB and NIR), and  $H, W$  the spatial dimensions of each image. When indexing a tensor with a single axis, we refer to its slice in the other dimension: eg  $x_t \in \mathbf{R}^{C \times H \times W}$  with  $t \in [1, T]$ . The PVTv2 model from Fogel et al. (2025) defines a mapping  $\psi_{\text{CHM}} : \mathbf{R}^{C \times H \times W} \mapsto \mathbf{R}_+^{H \times W}$ , that predicts a canopy height map from a single-year image. We applied  $\psi_{\text{CHM}}$  independently to each overlapping SPOT-6/7 image (See Section 2.1.2) of each year to obtain raw height predictions  $h_t = \psi_{\text{CHM}}(x_t)$ . We then averaged the predicted values for overlapping images to obtain a single country-wide prediction per year.

The high variability in SPOT-6/7 images due to different acquisition conditions (angle, time of the year, aerosols) and registration errors introduces temporal and spatial inconsistencies in the predicted dataset that we addressed by applying a series of post-processing steps described below.

### 2.2.2. Co-Registration

To correct for small spatial misalignments between annual predictions, we aligned each yearly map  $h_t$  to a reference map  $h_0$  corresponding to the year 2019, as it represents the middle of the time-series. Let  $\mathcal{O}$  be a discrete set of integer offsets, corresponding to a  $5 \times 5$  window centered at zero (i.e.,  $\pm 2$  pixels in each direction). We selected the optimal offset  $o_t^*$  by minimizing the squared difference:

$$o_t^* = \operatorname{argmin}_{o \in \mathcal{O}} \sum_{h,w} \left\| h_t(w + o_x, h + o_y) - h_0(w, h) \right\|^2$$

Each canopy map  $h_t$  was then shifted by the corresponding offset  $o_t^*$ . We applied this process by small patches of  $2000 \times 2000$  pixels. These patches were taken with an overlap ensuring that, after registration, each input pixel remains covered by at least one shifted patch. Registered predictions in the overlapping regions were then averaged to produce a seamless, registered time series of canopy height maps, which we denote by  $h \in \mathbf{R}^{T \times H \times W}$  in the following.

### 2.2.3. Time-series post-processing with total variation (TV) denoising.

In most cases, forest dynamics naturally evolve in a very structured way: canopy height increases slowly over time due to biological growth, whereas decreases are abrupt and associated with discrete events such as cuts, storms, wildfires, or individual mortality. Similarly, neighbour pixels tend to have similar heights over a forest stand. To mitigate the noise in our height time-series coming from various conditions of acquisition in SPOT-6/7 images and get closer to these forest characteristics, we applied a spatio-temporal total variation (TV) denoising scheme using the Chambolle-Pock primal-dual algorithm re-implemented in a GPU-compatible framework to enable efficient large-scale processing (Chambolle and Pock, 2011). The TV regularisation increases spatial coherence and forms temporally smooth, piecewise-constant trajectories while preserving the sharp drops that correspond to real disturbances.

For a data-cube  $g \in \mathbf{R}^{T \times H \times W}$  we define the total temporal variation of  $g$  as

$$\operatorname{TV}_{\text{temp}}(g) = \sum_{t=1}^{T-1} \|g_{t+1} - g_t\|$$

with  $T$  being the number of years ( $T = 11$ ), and the total spatial variations of  $g$  as

$$\operatorname{TV}_{\text{spat}}(g) = \sum_{h,w} \left( \|g_{h+1,w} - g_{h,w}\| + \|g_{h,w+1} - g_{h,w}\| \right)$$

The  $\|\cdot\|$  notation defines here the Frobenius norm of a tensor defined as  $\|A\| = \left( \sum_{i_1, i_2, \dots, i_N} A[i_1, i_2, \dots, i_N]^2 \right)^{\frac{1}{2}}$  for a tensor of dimension  $N$ , with  $A[i_1, i_2, \dots, i_N]$  being the value of the tensor at coordinates  $i_1, i_2, \dots, i_N$ . Given the registered predictions  $h$ , we estimated a denoised series  $g^*$  as the function  $g$  that minimizes the following expression:

$$g^* = \operatorname{argmin}_{g \in \mathbf{R}^{T \times H \times W}} \|h - g\|^2 + \lambda_{\text{temp}} \operatorname{TV}_{\text{temp}}(g) + \lambda_{\text{spat}} \operatorname{TV}_{\text{spat}}(g)$$

With  $\lambda_{\text{temp}}$  and  $\lambda_{\text{spat}}$  denoting the temporal and spatial regularization weights. After trial and error experiment, we set  $\lambda_{\text{temp}} = 5$  and  $\lambda_{\text{spat}} = 0.5$  in this study. We chose higher temporal regulation because stable height trajectories are essential for detecting disturbance events, whereas spatial consistency had already been largely enforced by the co-registration step, leaving only minor residual artifacts to correct. We refer to the resulting height time series as FORMSpOT (FOREst Mapping with Spot Time series).

### 2.2.4. Disturbance polygons

To validate FORMSpOT- $\Delta$  polygons, we derived reference disturbance polygons from diachronics 1m resolution ALS CHMs derived from acquisitions with at least 5 pts/m<sup>2</sup> (Fig. 3). Canopy disturbances were defined here as a change of more than 5 m in height at the pixel level and a minimum area of connected disturbed pixels of 10 m<sup>2</sup>. This definition included both the definition of canopy gaps, often defined as a decrease in canopy height below a given height threshold (Vepakomma et al., 2008), and canopy tree replacement, in which a dominant tree may be removed and replaced by a co-dominant or dominant one. There does not exist any universal definition of gaps in terms of height (White et al., 2018; Vehmas et al., 2011), but the 5 m threshold is often used to differentiate the understorey from the tree stratum. The same threshold was also adapted for

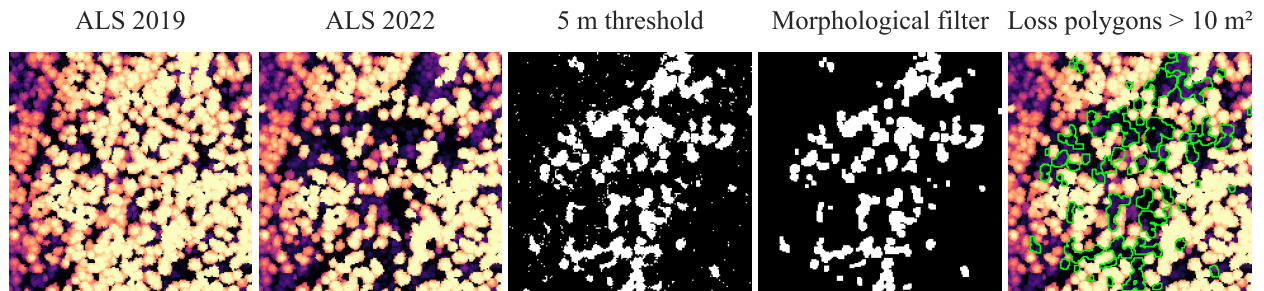


**Figure 3: Computing disturbance polygons.** We first computed the difference between two ALS-derived 1 m CHMs and applied a 5 m height-loss threshold to generate a binary disturbance mask. We then applied an opening morphological filter (Serra, 1982) to clean the mask. Finally, we retained all resulting polygons larger than  $10 \text{ m}^2$  as reference disturbance polygons.

tree replacement, considering the errors in height maps, to avoid false detections. While many papers have used area thresholds below  $10 \text{ m}^2$  to define a gap, we choose a  $10 \text{ m}^2$  value to both minimize false detection and allow comparison with other remote sensing products such as those derived from Sentinel 2 data. First, we applied a 5 m loss threshold between two ALS-derived CHMs to obtain a binary mask of disturbed pixels. Next, we removed small artifacts and regularized mask contours using an opening morphological filter (Serra, 1982): we successively applied binary erosion and dilation with a kernel size of 3 pixels. Finally, we converted the mask into polygons and filtered out those with an area lower than  $10 \text{ m}^2$ .

We used the same procedure for FORMSpOT maps to obtain FORMSpOT- $\Delta$  yearly forest loss polygons. For other height maps (e.g. Pauls and FORMS-T), we only applied a 5 m threshold since their 10 m resolution made filtering unnecessary. For the fractional tree cover map of deadtrees.earth, we chose a 25% tree cover loss threshold, without using a morphological filter for the same reason. For the SUFOSAT forest clear-cut polygons, which are provided along with a specific date of disturbance, we included all polygons with a date between the two ALS acquisitions. For other datasets that only provide a year of disturbance (e.g. Hansen, Turubanova, EFDA), we included all the polygons marked with a year between the first ALS year (excluded) to the second ALS year. The resulting polygons were filtered using a forest mask (IGN, 2025b) to restrict our analysis to forest areas only.

### 2.2.5. Metrics

#### *Area-based disturbance metrics compared to ALS data.*

We evaluated FORMSpOT- $\Delta$  against ALS-derived polygons by computing detection metrics within disturbance size classes (e.g.,  $10\text{-}100 \text{ m}^2$ ,  $100\text{-}1000 \text{ m}^2$ ,  $0.1\text{-}1 \text{ ha}$ ,  $>1 \text{ ha}$ ) as well as over the full set of polygons. We

computed all metrics using an area-based formulation. Precision measures the ratio between the total overlap area (predicted  $\cap$  reference) and the total area of predicted polygons. Recall measures the ratio between the total overlap area and the total area of reference polygons. The F1-score takes the harmonic mean of precision and recall. We also computed metrics for disturbances within a set range of area (e.g.,  $10\text{-}100 \text{ m}^2$ ,  $100\text{-}1000 \text{ m}^2$ ,  $0.1\text{-}1 \text{ ha}$ ,  $>1 \text{ ha}$ ). The precision was computed using only the predicted polygons within the target range. For example, for the  $10\text{-}100 \text{ m}^2$  bin, precision corresponds to the intersection area between predicted polygons of that size and all reference polygons, divided by the total area of predicted polygons of that size. Conversely, we computed recall for the  $10\text{-}100 \text{ m}^2$  bin as the intersection area between all predicted polygons and the reference polygons of that size, divided by the total area of reference polygons of that size. Additionally, we computed the intersection over union (IoU), an overall metric of spatial agreement, to further evaluate the performance of the FORMSpOT- $\Delta$  polygons over a specific area (Fig. 6).

#### *Disturbance detection metrics compared to NFI data.*

In addition to the ALS-based evaluation, we compared the predicted polygons of FORMSpOT- $\Delta$  with disturbance information from the 2018-2023 French NFI plot revisits. We defined a plot as disturbed if at least one tree was cut or had been windthrown (dead or alive) in the five-year (2018-2023) period. Standing dead trees were not considered disturbances, as they do not represent an actual loss of canopy height. However, their presence may still influence our height predictions, since the model was trained on ALS data, which are sensitive to standing dead trees (Heinero et al., 2023). Each NFI plot from the 2018-2023 campaign (5,087) was assigned to one of four categories: true positive (TP): disturbed plot intersecting a disturbed FORMSpOT- $\Delta$  poly-

gon, with the disturbance arising at some point during 2018–2023, true negative (TN): undisturbed plot with no intersection, false positive (FP): undisturbed plot intersecting a polygon, and false negative (FN): disturbed plot intersecting no predicted polygon. Based on these categories, we computed precision (P), recall (R), and F1-score (F1) as follows  $P = \frac{TP}{TP+FP}$ ,  $R = \frac{TP}{TP+FN}$ ,  $F1 = \frac{2 \times P \times R}{P+R}$ . We also computed the recall as a function of disturbance magnitude to assess the minimum disturbance detectable by FORMSpOT- $\Delta$ . Disturbance magnitude was defined as the percentage of trees lost between 2018 and 2023: a value of 100% corresponds to a clear-cut, whereas a value of 10% reflects a low-

intensity disturbance. Equivalent analyses were conducted using basal area loss and by focusing on larger trees only (diameter at breast height greater than the plot-level mean). As these alternative formulations led to similar patterns, the simpler tree-count-based metric was retained. We carried out the same analysis for other disturbance products available for the 2018–2023 time period (e.g., Hansen, EFDA, FORMS-T, SUFOSAT).

### 3. Results

#### 3.1. Qualitative results

The FORMSpOT product provides 1.5 m forest height maps for France over an 11-year period,

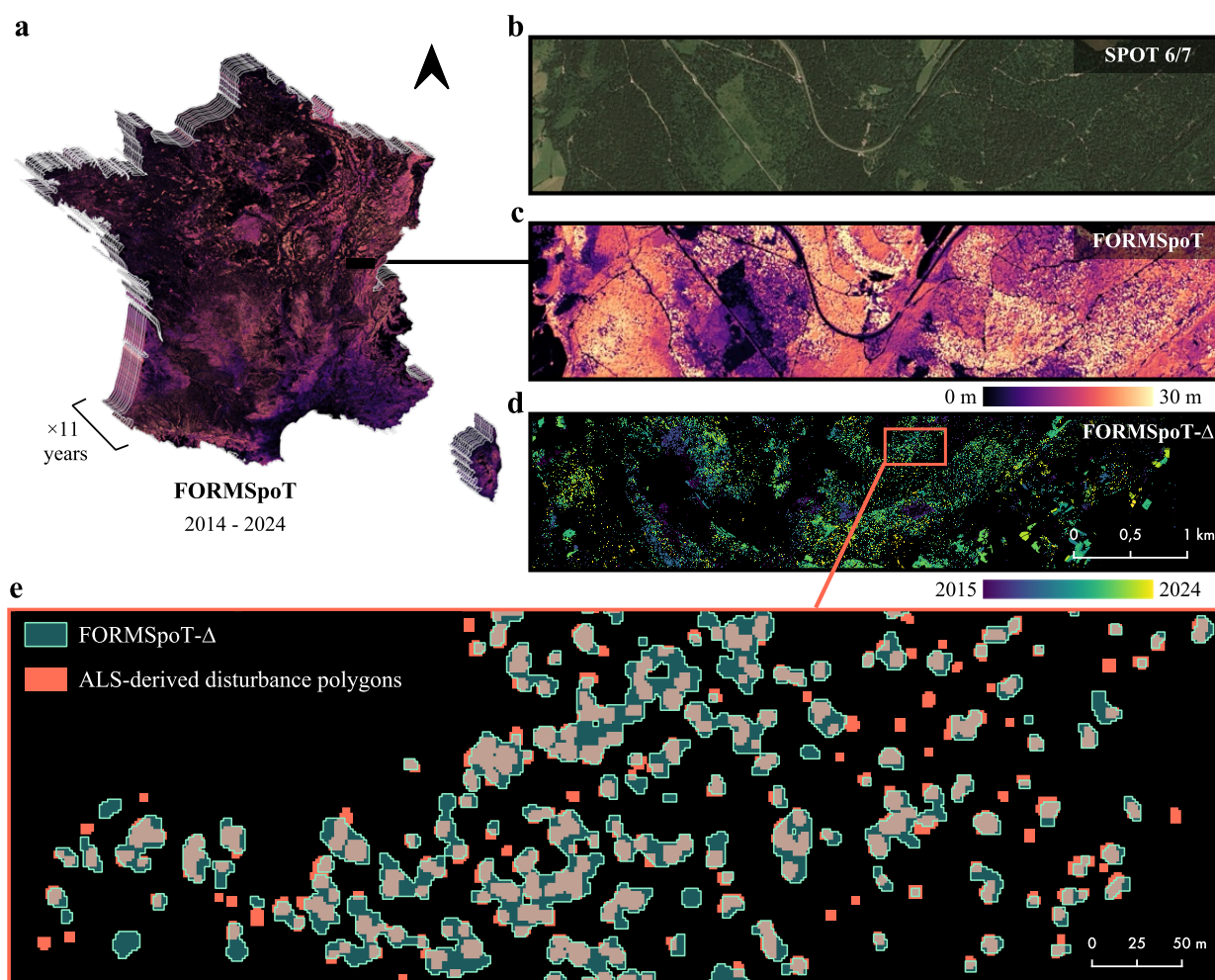


**Figure 4: Qualitative evaluation of FORMSpOT height maps and FORMSpOT- $\Delta$  polygons.** a) The FORMSpOT maps at 1.5 resolution derived from SPOT-6/7 imagery with the PVTv2 transformer model trained on ALS data. b) Closer view of a SPOT-6/7 image (2022) over the Jura mountains. c) FORMSpOT predicted height (2022) at 1.5 m resolution over this area. Brighter colors indicate higher heights. d) FORMSpOT- $\Delta$  disturbance polygons derived from the FORMSpOT height time series over this area. Brighter colors indicate more recent forest disturbances. e) Comparison of ALS-derived disturbance polygons from successive acquisitions (2019–2022) with FORMSpOT- $\Delta$  polygons spanning these years.

while FORMSpOT- $\Delta$  delivers a tree-level disturbance database. Both products can be freely accessed at <https://doi.theia.data-terra.org/FORMSpOT/>. Fig. 4 illustrates examples of these datasets together with the corresponding SPOT-6/7 image. Despite variability in acquisition conditions, the FORMSpOT series remains highly consistent over time, owing to the temporal denoising procedure (Section 2.2.3). A detailed visualization of the TV denoising effect is provided in Appendix A.

### 3.2. Height validation with NFI

We validated the FORMSpOT height maps by comparing them to the corresponding-year height measurements from French NFI plots (see Section 2.1.4). Fig. 5.a and Fig. 5.b present the aggregated validation over all years, while Fig. 5.c reports the annual mean absolute error (MAE) and coefficient of determination ( $r^2$ ). Overall, FORMSpOT achieved an  $r^2$  of 0.74 and a MAE of 3.85 m. Lower canopy heights were well reproduced, with minimal bias (e.g., 0.70 m in the 10–15 m range), whereas higher canopy classes showed a larger negative bias (e.g., -9.8 m in the 35–40 m range). The

yearly MAE remained relatively stable (standard deviation SD = 0.08 m), ranging from 3.71 m in 2014 to 4.99 m in 2023. The  $r^2$  values also showed limited interannual variability (SD = 0.02, spanning from 0.70 in 2014 to 0.76 in 2020 and 2022).

### 3.3. ALS-based validation of FORMSpOT- $\Delta$ polygons

In Fig. 6, we illustrate disturbance polygons from all datasets alongside FORMSpOT- $\Delta$  and ALS-derived polygons for the Jura site. This visualization underscores the importance of very high spatial resolution for accurate disturbance detection. In addition to large clear-cut areas, the ALS-derived polygons also reveal numerous tree-sized disturbances associated with selective logging or salvage operations following bark beetle outbreaks, which are frequent in this region. FORMSpOT- $\Delta$  closely reproduced these fine-scale patterns, capturing disturbances down to individual trees, whereas lower-resolution products primarily detected only large harvesting events. This is reflected in the IoU values computed against ALS-derived polygons: FORMSpOT- $\Delta$  achieved an IoU of 0.64, which is 45%

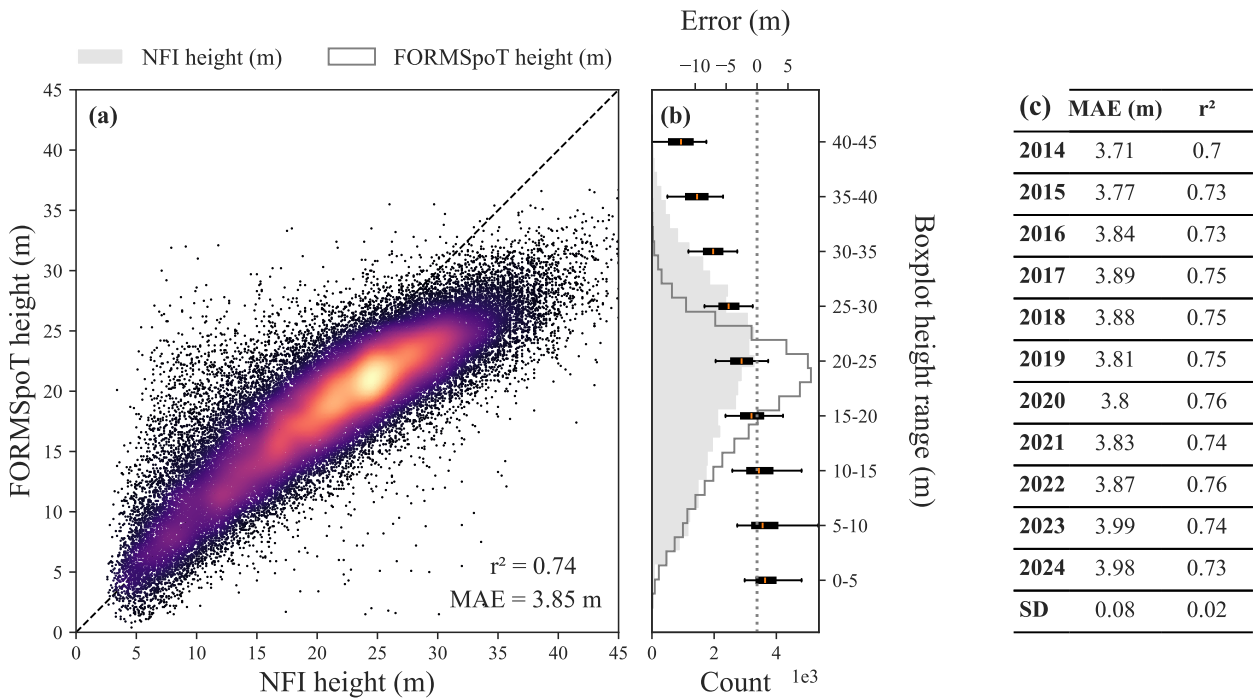


**Figure 5: Validation of FORMSpOT canopy height estimates using NFI field plots across 11 years.** (a) Density plot of FORMSpOT-predicted height versus NFI reference height (see Section 2.1.4), with brighter colors indicating higher point density. The dashed line represents the 1:1 relationship. (b) Histogram with boxplots showing the distribution of height differences within 5 m reference height bins. The red line denotes the median, the box edges indicate the lower and upper quartiles, and the whiskers represent the 5th and 95th percentiles. (c) Table reporting the mean absolute error (MAE) and the coefficient of determination ( $r^2$ ) for all years (2014–2024). The standard deviation (SD) across years is shown in the last row.

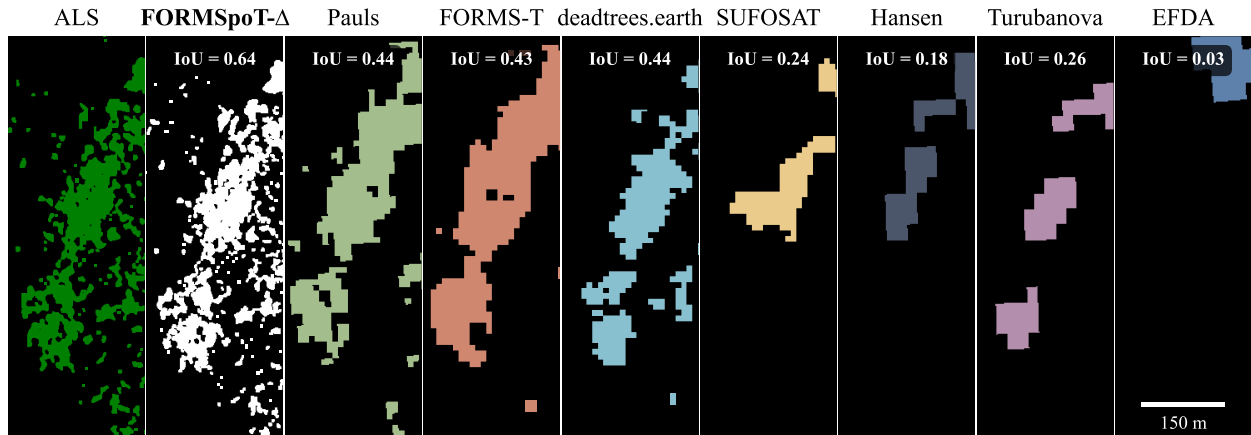


**Figure 6: Visual comparison of disturbance polygons at the Joux-Fresse site (2019-2022).** ALS-derived polygons were derived using a 5 m threshold (See Section 2.2.4). The Turubanova dataset is only available for the 2019-2021 period, but is shown for reference. Intersection over union (IoU) values are displayed for this specific area (46.83 N,6.01 E).

higher than the second-best datasets (Pauls and deadtrees.earth), whose IoU is 0.44.

Fig. 7 shows precision and recall (Fig. 7.a) as a function of disturbance size for FORMSpOT- $\Delta$  and the other available datasets in the Joux-Fresse site, where two ALS acquisitions (2019 and 2022) provide reference disturbances. FORMSpOT- $\Delta$  outperformed all datasets across all disturbance-size classes. Notably, it was the only product capable of predicting 10–100 m<sup>2</sup> disturbances, for which it obtained a precision of 0.58, enabled by its 1.5 m spatial resolution (Fig. 7.b). These small disturbances could occasionally be detected by other datasets, but only within larger polygons (Fig. 7.c), and their recall remained substantially lower: FORMSpOT- $\Delta$  detected twice as many small disturbances (recall = 0.38) as the second-best model (Pauls, recall = 0.15). For larger disturbances (>1 ha), FORMS-T (recall = 0.90), Pauls (recall = 0.90) and deadtrees.earth (recall = 0.89) achieved recall values comparable to FORMSpOT- $\Delta$  (recall = 0.95), but with much lower precision, indicating systematic overestimation of disturbed area. In contrast, FORMSpOT- $\Delta$  more accurately matched the ALS polygon boundaries, with a precision of 0.73 for disturbances greater than 1 ha, compared to the second-best dataset (deadtrees.earth), which achieved only a precision of 0.61.

In Fig. 7.d, we sorted the disturbance polygons predicted by each dataset by size and computed the cumulative precision and recall. FORMSpOT- $\Delta$  performed best overall: it reached the highest final recall (0.69) while keeping the highest precision across the full recall range. Pauls had the second-highest final recall

(0.46), but its precision stayed below that of all other datasets, reflecting strong overprediction and many false positives. Hansen showed relatively good precision but a low final recall (0.20), meaning that the polygons it identified were often correct, but most disturbances remained undetected.

We compared the disturbance polygons from FORMSpOT- $\Delta$  with ALS-derived disturbance polygons obtained from successive ALS acquisitions (Section 2.1.3) across 19 sites. We present six of them in Fig. 8. Additional validation can be found in the supplementary materials. For each site, we computed precision, recall, and F1-scores, and performed the same evaluation for other existing disturbance products (Section 2.1.5).

Across all sites, FORMSpOT- $\Delta$  consistently outperformed the other models, showing substantially higher F1-scores. At the Landes site, a maritime pine plantation characterized by intensive management and clearcuts (disturbances >0.1 ha, accounting for 72% of the total disturbed area), most datasets achieved relatively high performance, with F1-scores above 0.4, except for EFDA. Even in this context, FORMSpOT- $\Delta$  remained the top-performing method, reaching an F1-score of 0.76. In contrast, performance drops sharply in more structurally complex forests. At the Chantilly site, a broadleaf forest dominated by declining oak stands that undergo salvage logging, FORMSpOT- $\Delta$  was the only product achieving an F1-score above 0.1, with a value of 0.39. Similarly, in high mountainous areas, such as the Barousse site, in the Pyrenees mountains, where 69.5% of the disturbed area occur in polygons smaller than 100 m<sup>2</sup>, FORMSpOT- $\Delta$  was the only dataset capable of

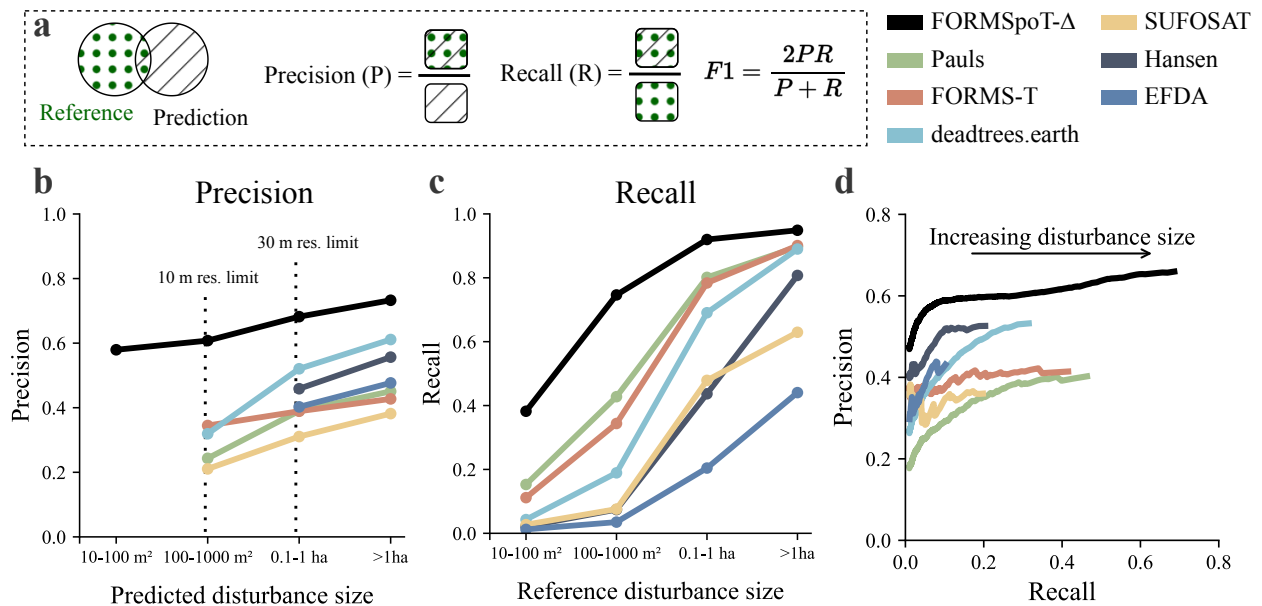


**Figure 7: Validation of FORMSpOT-Δ on the Joux-Fresse site and comparison with existing disturbance products.** a) Illustration of precision, recall, and F1-score. b) Precision and c) recall by disturbance size class. For precision, size classes refer to the predicted polygons; for recall, they refer to the ALS-derived reference polygons. Limits below which 10 m and 30 m resolution products cannot predict polygons are indicated. No such limit is shown for recall, since products can detect small disturbances even when represented by larger polygons. e) Precision–recall curves. Predicted disturbance polygons were ranked by ascending area. Precision and recall were then evaluated iteratively as polygons were added to the dataset.

achieving a high F1-score of 0.45, which is 9 times the score of the second best dataset (Pauls, with a F1 score of 0.05). Apart from FORMSpOT-Δ, the best-performing datasets were Pauls, deadtrees.earth, and FORMS-T, all based on Sentinel-1/2 imagery at 10 m resolution and therefore unavailable before 2018. Landsat-based products showed noticeably lower performance. Among them, Hansen (F1 = 0.20 for the Vosges site) outperformed EFDA (F1 = 0.14). SUFOSAT, designed for submonthly clear-cut monitoring rather than annual disturbance mapping, achieved intermediate performance, with F1-scores generally similar to EFDA (F1 = 0.11) at the Vosges site.

### 3.4. NFI-based validation of disturbance polygons

We validated the predicted disturbance polygons with repeated plot-level NFI measurements as reference data. We selected plots measured in 2018 and 2023, and compared the reported disturbance status with predicted disturbance polygons (Fig. 9).

FORMSpOT-Δ achieved the highest F1-score (0.44), compared with 0.27 for FORMS-T, 0.21 for Hansen, 0.20 for EFDA, and 0.20 for SUFOSAT (the other datasets do not cover the 2018–2023 period). This higher F1-score comes from a higher recall value

(0.33), which was twice that of the second-best dataset, FORMS-T (0.16): FORMSpOT-Δ identified twice as many disturbed plots. Its precision was slightly lower than the highest one (0.67 vs. 0.80 for SUFOSAT), meaning that 67% of plots intersecting a FORMSpOT-Δ polygon in 2018–2023 were confirmed as disturbed in the field. To demonstrate the advantage of FORMSpOT-Δ in detecting small disturbances, we classified NFI plots by disturbance magnitude and calculated the fraction of plots detected by each dataset for each class, corresponding to recall values per disturbance magnitude. FORMSpOT-Δ outperformed all other datasets across all classes and showed a notably higher rate of detection for small disturbances. For example, it detected 37% of plots with 30–40% of trees disturbed, which was 4 times more than the second-best model, EFDA, which detected only 9% of these plots. FORMSpOT-Δ could even identify 12% of nearly undisturbed plots (0–10% of trees disturbed over five years), while other datasets detected at most 3% (FORMS-T) of them.

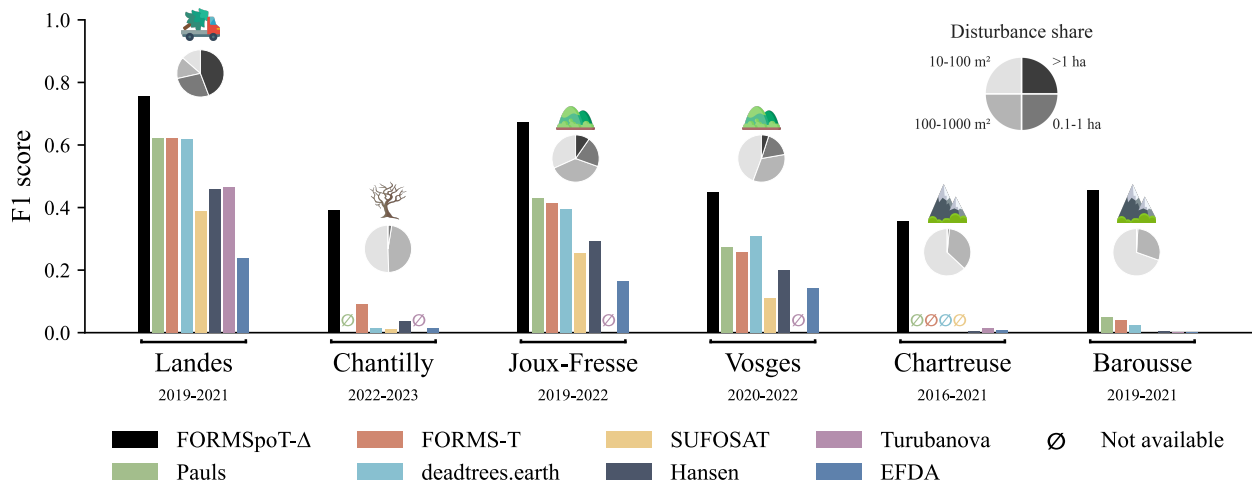


**Figure 8: F1-scores across the main validation sites.** Datasets that could not be evaluated at a given site because their acquisition dates did not match the ALS revisit period are marked with  $\emptyset$ . For each site, the proportion of disturbance size classes, expressed as a percentage of the total disturbed area derived from ALS polygons, is shown above the plot. From left to right, the symbols correspond to a heavily managed maritime pine plantation, a declining oak forest with salvage logging, a low-mountain mixed forest, and high-mountain mixed forest with selective logging.

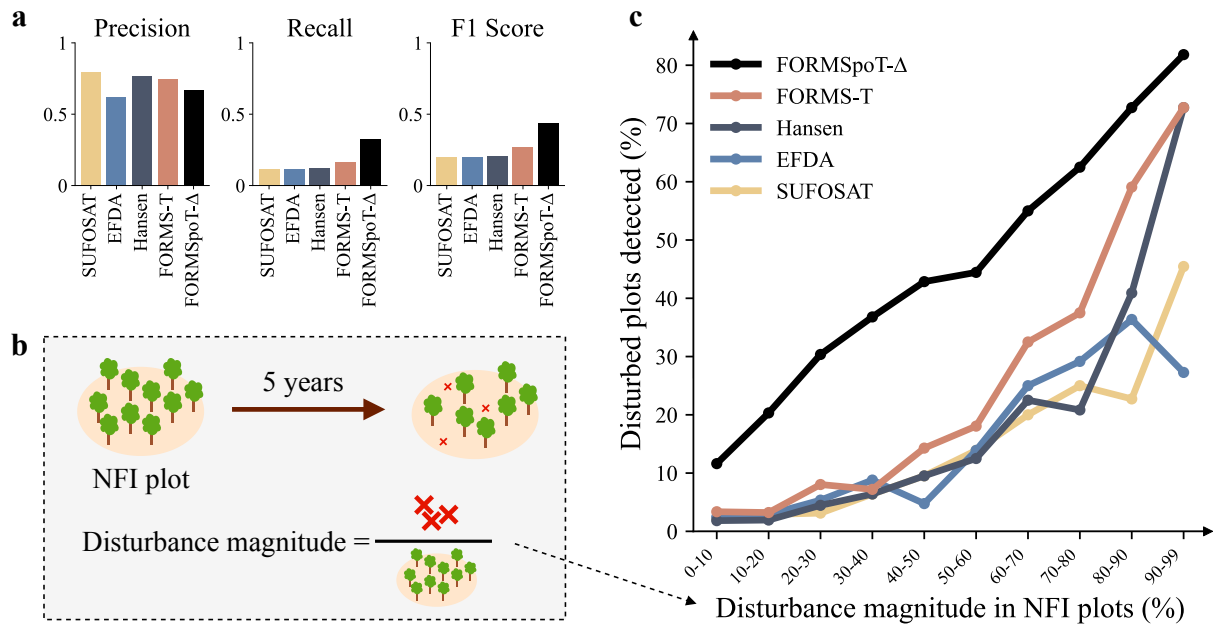


**Figure 9: Comparison with field-measured disturbances from French NFI plots.** a) Precision, recall, and F1-scores for FORMSpOT- $\Delta$  and four other products (SUFOSAT, EFDA, Hansen, FORMS-T) using NFI disturbance information from the 2018–2023 revisit cycle. b) Illustration of NFI plot revisits and computation of disturbance magnitude, defined as the percentage of measurable trees recorded as disturbed over the 5-year interval. c) Recall per disturbance-magnitude class, measured as the fraction of NFI plots intersecting a predicted disturbance polygon.

## 4. Discussion

### 4.1. Detecting small disturbances requires high resolution

Very high-resolution forest monitoring opens new opportunities for ecological and forestry applications. Liu et al. (2023) used Planet imagery to map trees outside forests across Europe, revealing patterns that coarser-resolution sensors cannot capture. Tucker et al. (2023), using Maxar imagery, estimated carbon stocks of isolated trees in African drylands, features previously undetectable from space. In line with these previous examples, FORMSpOT provides annual, country-wide forest monitoring at 1.5 m resolution, far beyond what is achievable with Sentinel-1/2 or Landsat-based products. Thanks to the finer resolution of SPOT-6/7 imagery, our approach captures small disturbances down to the scale of individual trees (Section 3.1). While Fig. 8 shows that FORMSpOT- $\Delta$  achieves the highest overall F1-scores across all compared datasets, the advantage becomes particularly striking when focusing on small-scale disturbances. For instance, in mountainous areas (e.g., Barousse, Chartreuse), where small-scale disturbances dominate due to selective logging, FORMSpOT- $\Delta$  is the only dataset that detects a large proportion of disturbance with F1-scores an order of magnitude higher than other products.

Across all sites, after FORMSpOT- $\Delta$ , the strongest results are obtained from products based on Sentinel-2 imagery combined with deep learning methods (Pauls, deadtrees.earth, and FORMS-T). This is mainly due to the finer spatial resolution of Sentinel-2 at 10 m (compared to Landsat at 30 m), which enables a more precise detection of small disturbances. The performance may also benefit from the use of deep learning architectures, such as convolutional networks in FORMS-T and Pauls, and vision transformers in deadtrees.earth. These products outperform Landsat-based datasets (Hansen, EFDA, Turubanova), which are yet specifically designed to retrieve disturbances. Indeed, the 30 m native resolution of Landsat prevents the detection of disturbances smaller than roughly 0.1 ha.

Although deadtrees.earth uses UAV-derived labels for fractional tree cover and Pauls and FORMS-T predict canopy height from GEDI, their disturbance detection performance is similar. This suggests that all three are limited by the 10 m resolution of Sentinel-2 imagery, indicating that resolution could be the primary driver of disturbance detection performance, rather than the choice of deep learning architecture or training data.

### 4.2. Applications and perspectives for forest monitoring

The high-resolution FORMSpOT- $\Delta$  polygons make it possible to detect subtle changes in forest height that remain invisible to coarser sensors. This level of detail can serve as a spatial indicator of forest management practices. While clearcuts are detectable with 10-30 m resolution imagery, higher resolution could potentially enable the identification of thinning, selective logging, and even patterns associated with coppice systems (Evans, 1992) or even-aged and uneven-aged stands (Nolet et al., 2018). Such information is important to adapt forest practices to climate change, as management practices, such as thinning, are thought to influence forest resilience (Moreau et al., 2022). Although some of these patterns can already be inferred from NFI plot revisits, remote sensing complements sparse field data with spatially continuous predictions. Fig. 10 illustrates this potential by showing, for each forest region (IGN, 2010), the share of total disturbed area within different disturbance-size classes. Distinct practices emerge across regions: large disturbances dominate in the Landes (southwest), where clearcut management is common, whereas mountain regions and southern France show a larger proportion of small disturbances, consistent with more selective or irregular silvicultural practices. Such maps can also serve as a proxy to monitor forest fragmentation and management policies. In France, forest ownership is largely composed of small, fragmented private parcels. The drivers and patterns of forest management remain poorly understood, which constrains the capacity of public authorities to develop and implement policies aimed at enhancing forest management in the context of climate change mitigation and adaptation. The availability of high-resolution, annual disturbance data offers the opportunity to better link management practices with ecological and economic contexts, thereby informing and guiding evidence-based public decision-making. FORMSpOT- $\Delta$  can also support studies focused on small-scale forest disturbances. For example, Krüger et al. (2024) analysed gap expansion using successive ALS acquisitions over a national park in Germany. While our satellite-based approach cannot match the level of detail provided by ALS, it can extend these analyses by offering longer time series and regular updates at a much lower cost than repeated ALS campaigns. Such time series could also help detect mortality in young forest plantations and alert managers when no growth is observed during the first years after planting. This is particularly important because many carbon-offset programs, such as the French Label Bas Carbone, rely on these plantations, making reliable monitoring tools essential. In 2022, for example, the French

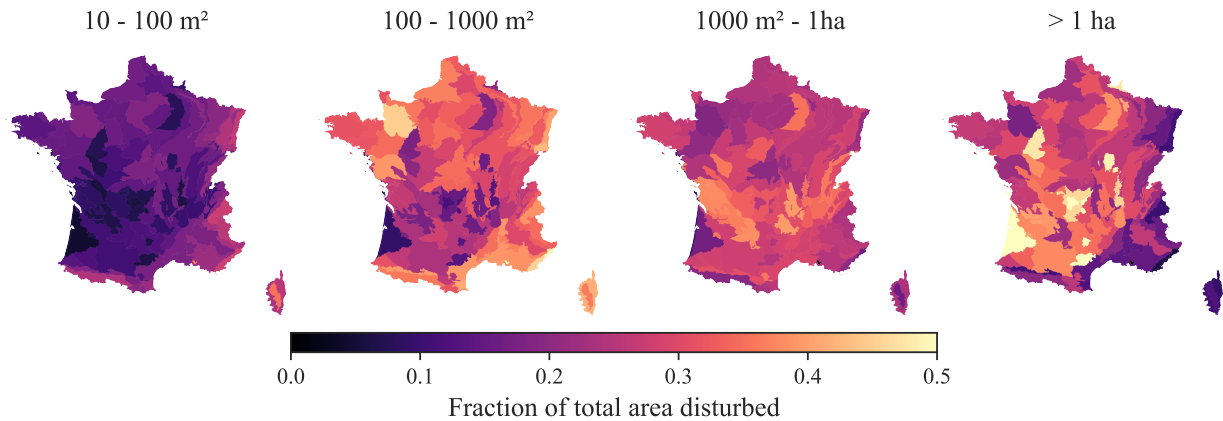


**Figure 10: Relative importance of disturbance size per region.** For each class of disturbance area in FORMSpOT- $\Delta$ , we represent the fraction of disturbed area relative to the total disturbed area (mean over 2014-2024).

Department for Forest Health (DSF, 2023) reported that 38% of young plantations failed due to a combination of biotic and abiotic stresses, underscoring the need for systematic, scalable monitoring.

#### 4.3. Limitations and path to improvements

The inherent SPOT-6/7 variability and acquisition conditions make FORMSpOT predictions uncertain in specific areas. Particularly, the 2024 image acquired on the 9th of June over the eastern part of Corsica has high cloud cover, which affects the precision of our height predictions. Additionally, some images were acquired in winter with a snow coverage that can lead to erroneous height predictions and disturbance polygon detection. The TV denoising process (See Section 2.2.3) used to stabilize the time series improves the temporal consistency of the height predictions and removes unwanted variability due to acquisition conditions of SPOT-6/7 imagery. However, it may erase or attenuate abrupt changes like forest clearcutting, particularly at the extremities of the time series (2014 or 2024). In addition, this regularization tends to smooth subtle long-term trends such as forest growth, which therefore cannot be evaluated with this dataset.

The PVTv2 model from Fogel et al. (2025) was trained on pairs of SPOT-6/7 images and ALS-derived canopy heights collected across all seasons. This allows the model to predict forest heights from imagery acquired at any time of the year. However, the SPOT-6/7 images and ALS data were matched only by year, not by month, which can lead to temporal misalignments during training. As a result, seasonal phenology may still affect height predictions. Further research to improve the predictions could include spatio-temporal models,

that directly predict consistent height time-series from a temporal data-cube.

In this study, we derived disturbance polygons from several products not originally designed for this purpose. SUFOSAT, based on 10 m Sentinel-1 imagery, is designed for submonthly detection of forest clearcuts. A yearly comparison including small-scale disturbances does not reflect its intended use, but it was included in this study for reference. For deadtrees.earth, we applied a 25% fractional tree cover loss threshold to its 10 m Sentinel-2 data. While this sets a practical detection limit at the pixel scale (100 m<sup>2</sup>), smaller disturbances could theoretically be detected. For example, a 30% loss within a 100 m<sup>2</sup> pixel could correspond to roughly 30 m<sup>2</sup> of disturbed area, though the exact location cannot be resolved. For Pauls and FORMS-T, we applied a 5 m height-loss threshold to their height maps, but these products were primarily developed for canopy height mapping rather than disturbance detection. These limitations should be considered when comparing their performance to FORMSpOT- $\Delta$ , which was specifically designed for high-resolution disturbance detection.

The evaluation metrics we use are area-based, which are particularly strict: if a small tree-level disturbance is detected but the polygon contours do not perfectly match the reference, the resulting score can be substantially lower than one, even though the disturbance is captured. This explains why, in Fig. 7.c, large disturbances (>1 ha) show a recall of around 0.9 for FORMSpOT- $\Delta$ , FORMS-T, and Pauls, rather than a perfect 1.

Even though the methodology presented here is applicable globally, open access to SPOT-6/7 imagery is currently restricted to mainland France, and the SPOT mission is expected to be phased out in favor of the Pleiades constellation. The new Pleiades sensors offer sub-meter

resolution and could therefore provide the basis for future annual forest monitoring products in France.

## 5. Conclusion

In this work, we presented a full workflow to generate very high-resolution canopy height maps and disturbance polygons across France from eleven years of SPOT-6/7 imagery. We applied the PvTv2 hierarchical transformer model, pretrained on the Open-Canopy dataset (Fogel et al., 2025), to a nationwide coverage of SPOT-6/7 images and produced annual 1.5 m canopy height maps. Because SPOT-6/7 acquisitions vary in geometry and atmospheric conditions, we introduced a post-processing chain that combines CHM co-registration and total-variation denoising to stabilize the height time series and obtain FORMSpOT. From this time series, we extracted disturbance polygons for the 2014–2024 period, resulting in FORMSpOT- $\Delta$ , which captures changes down to the scale of individual trees.

We assessed FORMSpOT- $\Delta$  using successive ALS revisits, allowing tree-level validation, and French NFI plot revisits. In both cases, FORMSpOT- $\Delta$  outperformed existing disturbance datasets, especially for small events, with detection rates up to an order of magnitude higher than current products. This fine-scale information helps reveal patterns that were previously missed and opens new possibilities for forestry applications: tracking the outcome of young plantations, mapping management practices such as thinning or selective logging, and improving estimates of carbon losses from subtle disturbances.

Both FORMSpOT and FORMSpOT- $\Delta$  are openly available at <https://doi.theia.data-terra.org/FORMSpOT/>, making them accessible to a wide range of forestry stakeholders. Looking ahead, these datasets can support more responsive forest monitoring and help guide management strategies in a context of climate change.

## 6. Acknowledgements

We acknowledge all contributors to this work. Access to the Chantilly ALS acquisition was provided by Laurent Saint-André and the group Ensemble sauvons la forêt de Chantilly. ALS data were also provided by the Office National des Forêts (ONF), with coordination by Jérôme Bock. The Massif des Bauges LiDAR dataset was funded by ADEME through the GRAINE program (PROTEST project 1703C0069), the Jura-Doubs dataset by the Conseil Régional Bourgogne Franche-Comté,

and the Chartreuse dataset by ONF, PNR de Chartreuse, and INRAE. We thank DINAMIS and Airbus for open access to SPOT-6/7 imagery, the French National Forest Inventory foresters for field data collection, and IGN for nationwide access to LiDAR HD data. This work is part of the ALAMOD project (FairCarboN) funded by ANR under France 2030 (ANR-22-PEXF-0002), with additional support from PEPR FORESTT “Forest Resilience” (ANR-24-PEFO-0003), AI4FOREST (ANR-22-FAI1-0002-01), TOSCA CFOREST 50M, SHARP (PEPR IA, ANR-23-PEIA-0008), the ARTEMIS program of Lorraine Université d’Excellence (ANR-15-IDEX-04-LUE), Hi! PARIS (ANR-23-IACL-0005), the EU Horizon Europe program (Grant No. 101131841), and the Swiss State Secretariat for Education, Research and Innovation (SERI). Computational resources were provided by IDRIS under the HPC allocations 2024-AD010114718 and 2025-AD010114718R1 granted by GENCI. Finally, we thank Flaticon.com for the icons used in Fig. 8 and Table 1.

## Appendix A. Effect of TV Denoising on height predictions

To ensure spatial and temporal consistency in the FORMSpOT height time series, we applied a spatio-temporal denoising algorithm (see Section 2.2.3). Fig. A.11 illustrates its effect on a specific location: before denoising, the series shows large fluctuations caused by changing SPOT-6/7 acquisition conditions, while after denoising, the height becomes stable and coherent through time. This consistency is essential for downstream analyses such as disturbance detection based on abrupt height changes.

Supplementary materials can be accessed at [https://drive.google.com/file/d/1C33jddTYH2PpP\\_cUbpjzjunWrOZLOfAU/view?usp=sharing](https://drive.google.com/file/d/1C33jddTYH2PpP_cUbpjzjunWrOZLOfAU/view?usp=sharing)

## References

- Ali, H., Mohammadi, J., Shataee Jouibary, S., 2024. Deep and machine learning prediction of forest above-ground biomass using multi-source remote sensing data in coniferous planted forests in Iran. *European Journal of Forest Research* 143, 1731–1745. URL: <https://doi.org/10.1007/s10342-024-01721-w>, doi:10.1007/s10342-024-01721-w.
- Ballère, M., Bouvet, A., Mermoz, S., Le Toan, T., Koleček, T., Bedeau, C., André, M., Forestier, E., Frison, P.L., Lardeux, C., 2021. SAR data for tropical forest disturbance alerts in French Guiana: Benefit

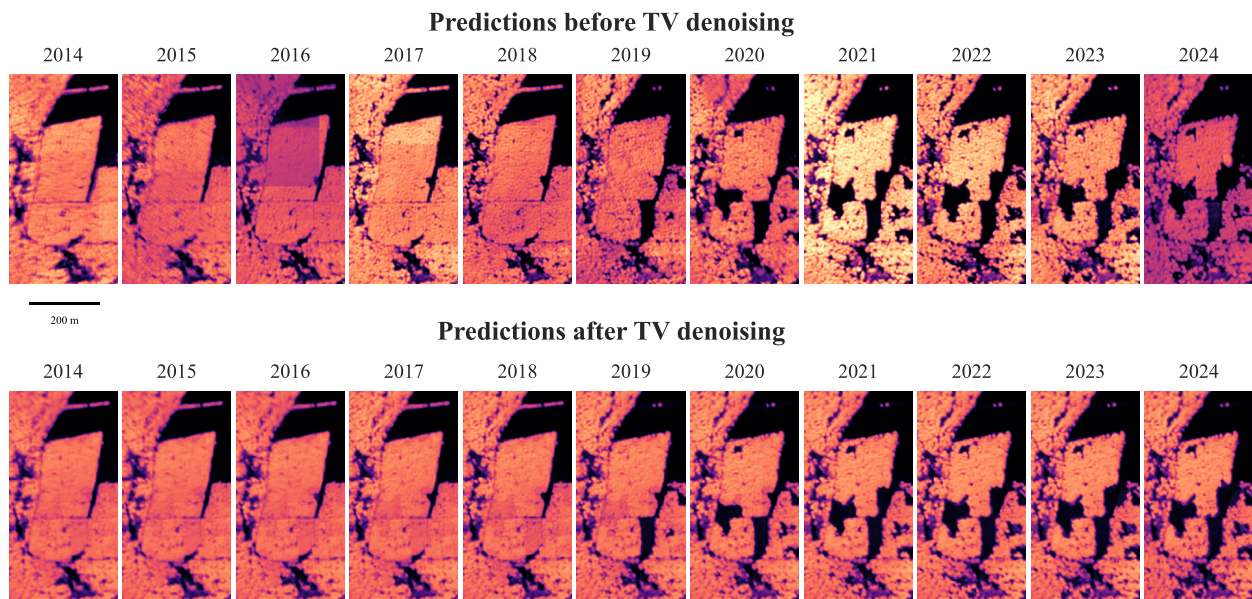


**Figure A.11:** Visual comparison of our height predictions before and after applying the TV denoising algorithm used as post-processing for the timeseries (location: 48.50 N, 7.14 E).

over optical imagery. *Remote Sensing of Environment* 252, 112159. URL: <https://linkinghub.elsevier.com/retrieve/pii/S0034425720305320>, doi:10.1016/j.rse.2020.112159.

Bontemps, J.D., Bouriaud, O., 2024. Take five: about the beat and the bar of annual and 5-year periodic national forest inventories. *Annals of Forest Science* 81, 53. URL: <https://doi.org/10.1186/s13595-024-01268-1>, doi:10.1186/s13595-024-01268-1.

Bossy, T., Ciais, P., Renaudineau, S., Wan, L., Ygorra, B., Adam, E., Barbier, N., Bauters, M., Delbart, N., Frappart, F., Gara, T.W., Hamunyela, E., Averti, I.S., Jaffrain, G., Maisongrande, P., Mugabowindekwe, M., Mugiraneza, T., Normandin, C., Obame, C.V., Peaucelle, M., Pinet, C., Ploton, P., Sagang, L.B., Schwartz, M., Sollier, V., Sonké, B., Tresson, P., De Truchis, A., Vo Quang, A., Wigneron, J.P., 2025. State of the art and perspectives for remote sensing monitoring of carbon dynamics in African tropical forests. *Frontiers in Remote Sensing* 6. URL: <https://www.frontiersin.org/journals/remote-sensing/articles/10.3389/frsen.2025.1532280/abstract>, doi:10.3389/frsen.2025.1532280. publisher: Frontiers.

Bouvet, A., Mermoz, S., Ballère, M., Koleck, T., Le Toan, T., 2018. Use of the SAR Shadowing Ef-

fect for Deforestation Detection with Sentinel-1 Time Series. *Remote Sensing* 10, 1250. URL: <https://www.mdpi.com/2072-4292/10/8/1250>, doi:10.3390/rs10081250. publisher: Multidisciplinary Digital Publishing Institute.

Brandt, M., Gominski, D., Reiner, F., Kariryaa, A., Guthula, V.B., Ciais, P., Tong, X., Zhang, W., Govindarajulu, D., Ortiz-Gonzalo, D., Fensholt, R., 2024. Severe decline in large farmland trees in India over the past decade. *Nature Sustainability* 7, 860–868. URL: <https://www.nature.com/articles/s41893-024-01356-0>, doi:10.1038/s41893-024-01356-0. publisher: Nature Publishing Group.

Breidenbach, J., McRoberts, R.E., Alberdi, I., Antón-Fernández, C., Tomppo, E., 2021. A century of national forest inventories – informing past, present and future decisions. *Forest Ecosystems* 8, 36. URL: <https://doi.org/10.1186/s40663-021-00315-x>, doi:10.1186/s40663-021-00315-x.

Cateau, E., Debaive, N., Drapier, N., Chantreau, F., Gilg, O., Laroche, F., Morin, X., Demets, V., Pimenta, R., Thompson, L., Paillet, Y., 2024. Tree inventory data from permanent plots in French forest reserves. *Ecology* 105, e4324. URL: <https://onlinelibrary.wiley.com/doi/abs/10.1002/ecy.4324>, doi:10.1002/ecy.4324. eprint: <https://esajournals.onlinelibrary.wiley.com/doi/pdf/10.1002/ecy.4324>.

- Chambolle, A., Pock, T., 2011. A First-Order Primal-Dual Algorithm for Convex Problems with Applications to Imaging. *Journal of Mathematical Imaging and Vision* 40, 120–145. URL: <https://doi.org/10.1007/s10851-010-0251-1>, doi:10.1007/s10851-010-0251-1.
- Cheng, Y., Oehmcke, S., Brandt, M., Rosenthal, L., Das, A., Vrieling, A., Saatchi, S., Wagner, F., Mugabowindekwe, M., Verbruggen, W., Beier, C., Horion, S., 2024. Scattered tree death contributes to substantial forest loss in California. *Nature Communications* 15, 641. URL: <https://www.nature.com/articles/s41467-024-44991-z>, doi:10.1038/s41467-024-44991-z. publisher: Nature Publishing Group.
- CLMS, 2023. Tree Cover Density 2023 (raster 10 m, 100 m), Europe, yearly. URL: <https://land.copernicus.eu/en/products/high-resolution-layer-forests-and-tree-cover/tree-cover-density-2023-raster-10-m-100-m-europe-yearly>.
- Collet, Y., Kucherawy, M., 2021. RFC 8878: Zstandard Compression and the 'application/zstd' Media Type. RFC Editor, USA.
- D'Amico, G., Vangi, E., Schwartz, M., Giannetti, F., Francini, S., Corona, P., Mattioli, W., Chirici, G., 2025. GEDI and Sentinel data integration for quantifying agroforestry tree height and stocks. *Journal of Environmental Management* 393, 127197. URL: <https://linkinghub.elsevier.com/retrieve/pii/S0301479725031731>, doi:10.1016/j.jenvman.2025.127197.
- DINAMIS, 2020. Couvertures nationales SPOT 6/7. URL: <https://theia.sedoo.fr/wp-content-theia/uploads/sites/6/2020/07/Usage-CouvNat.pdf>.
- DSF, 2023. Bilan de la réussite des plantations forestières de l'année. URL: <https://agriculture.gouv.fr/plantations-forestieres-2022-la-plus-mauvaise-annee>.
- Durrieu, S., Alleaume, S., De Boissieu, F., Dayal, K., Revers, F., TOPOLIDAR, 2025a. Données LIDAR ULM - Ripisylve du Ciron, printemps 2021. URL: <https://entrepot.recherche.data.gouv.fr/citation?persistentId=doi:10.57745/H0B5KL>, doi:10.57745/H0B5KL.
- Durrieu, S., Alleaume, S., De Boissieu, F., Dayal, K., Revers, F., UMR TETIS, 2025b. Données LIDAR ULM - Ripisylve du Ciron, automne 2019. URL: <https://entrepot.recherche.data.gouv.fr/citation?persistentId=doi:10.57745/GFEVRQ>, doi:10.57745/GFEVRQ.
- Espírito-Santo, F.D.B., Gloor, M., Keller, M., Malhi, Y., Saatchi, S., Nelson, B., Junior, R.C.O., Pereira, C., Lloyd, J., Frohking, S., Palace, M., Shimabukuro, Y.E., Duarte, V., Mendoza, A.M., López-González, G., Baker, T.R., Feldpausch, T.R., Brienen, R.J.W., Asner, G.P., Boyd, D.S., Phillips, O.L., 2014. Size and frequency of natural forest disturbances and the Amazon forest carbon balance. *Nature Communications* 5, 3434. URL: <https://www.nature.com/articles/ncomms4434>, doi:10.1038/ncomms4434. publisher: Nature Publishing Group.
- EU, 2024. The European Green Deal. URL: [https://ec.europa.eu/commission/presscorner/detail/en/fs\\_24\\_1391](https://ec.europa.eu/commission/presscorner/detail/en/fs_24_1391).
- Evans, J., 1992. Coppice forestry — an overview, in: Buckley, G.P. (Ed.), *Ecology and Management of Coppice Woodlands*. Springer Netherlands, Dordrecht, pp. 18–27. URL: [https://doi.org/10.1007/978-94-011-2362-4\\_2](https://doi.org/10.1007/978-94-011-2362-4_2), doi:10.1007/978-94-011-2362-4\_2.
- Fogel, F., Perron, Y., Besic, N., Saint-André, L., Pellissier-Tanon, A., Schwartz, M., Boudras, T., Fayad, I., d'Aspremont, A., Landrieu, L., Ciais, P., 2025. Open-canopy: Towards very high resolution forest monitoring, in: *Proceedings of the IEEE/CVF conference on computer vision and pattern recognition (CVPR)*, pp. 1395–1406.
- GDAL/OGR contributors, 2025. GDAL/OGR Geospatial Data Abstraction software Library. Open Source Geospatial Foundation. URL: <https://gdal.org>, doi:10.5281/zenodo.5884351.
- Hansen, M.C., Potapov, P.V., Moore, R., Hancher, M., Turubanova, S.A., Tyukavina, A., Thau, D., Stehman, S.V., Goetz, S.J., Loveland, T.R., Kommareddy, A., Egorov, A., Chini, L., Justice, C.O., Townshend, J.R.G., 2013. High-Resolution Global Maps of 21st-Century Forest Cover Change. *Science* 342, 850–853. doi:10.1126/science.1244693.
- Heinero, E., Tanhuanpää, T., Kukko, A., Hakala, T., Holopainen, M., 2023. Comparing field measurements and annotations as training data for UAV-based

- detection of standing dead trees in coniferous forest. *International Journal of Remote Sensing* 44, 5375–5396. URL: <https://doi.org/10.1080/01431161.2023.2248561>, doi:10.1080/01431161.2023.2248561. publisher: Taylor & Francis \_eprint: <https://doi.org/10.1080/01431161.2023.2248561>.
- Hertzog, L.R., Piedallu, C., Lebourgeois, F., Bouriaud, O., Bontemps, J.D., 2025. Turning point in the productivity of western European forests associated with a climate change footprint. *Science of The Total Environment* 967, 178843. URL: <https://www.sciencedirect.com/science/article/pii/S0048969725004784>, doi:10.1016/j.scitotenv.2025.178843.
- IGN, 2010. Sylvoécorégions. URL: <https://geo.data.gouv.fr/fr/datasets/a40c533b984bdcd33d8a38f2430a117672395bc0>.
- IGN, 2025a. LiDAR HD | Géoservices. URL: <https://geoservices.ign.fr/lidarhd>.
- IGN, 2025b. Masque Forêt v1. URL: <https://geoservices.ign.fr/bdforet>.
- IGN, 2025c. Mémento inventaire forestier IGN - 2025. URL: <https://www.calameo.com/read/0011885827c418636cbd4>.
- Korosuo, A., Pilli, R., Abad Viñas, R., Blujdea, V.N.B., Colditz, R.R., Fiorese, G., Rossi, S., Vizzarri, M., Grassi, G., 2023. The role of forests in the EU climate policy: are we on the right track? *Carbon Balance and Management* 18, 15. URL: <https://doi.org/10.1186/s13021-023-00234-0>, doi:10.1186/s13021-023-00234-0.
- Krüger, K., Senf, C., Jucker, T., Pflugmacher, D., Seidl, R., 2024. Gap expansion is the dominant driver of canopy openings in a temperate mountain forest landscape. *Journal of Ecology* 112, 1501–1515. URL: <https://onlinelibrary.wiley.com/doi/abs/10.1111/1365-2745.14320>, doi:10.1111/1365-2745.14320. \_eprint: <https://onlinelibrary.wiley.com/doi/pdf/10.1111/1365-2745.14320>.
- Lang, N., Schindler, K., Wegner, J.D., 2019. Country-wide high-resolution vegetation height mapping with Sentinel-2. *Remote Sensing of Environment* 233, 111347. URL: <https://www.sciencedirect.com/science/article/pii/S0034425719303669>, doi:10.1016/j.rse.2019.111347.
- Le Bouler, H., 2023. Ensemble Sauvons la forêt de Chantilly. Une recherche action collective de territoire face à un dépérissement forestier massif. *Revue forestière française* 74, 165–175. URL: <https://revueforestierefrancaise.agroparistech.fr/article/view/7590>, doi:10.20870/revfrrfr.2023.7590.
- Li, W., Niu, Z., Liang, X., Li, Z., Huang, N., Gao, S., Wang, C., Muhammad, S., 2015. Geostatistical modeling using LiDAR-derived prior knowledge with SPOT-6 data to estimate temperate forest canopy cover and above-ground biomass via stratified random sampling. *International Journal of Applied Earth Observation and Geoinformation* 41, 88–98. URL: <https://linkinghub.elsevier.com/retrieve/pii/S0303243415001063>, doi:10.1016/j.jag.2015.04.020.
- Liu, S., Brandt, M., Nord-Larsen, T., Chave, J., Reiner, F., Lang, N., Tong, X., Ciais, P., Igel, C., Pascual, A., Guerra-Hernandez, J., Li, S., Mugabowindekwe, M., Saatchi, S., Yue, Y., Chen, Z., Fensholt, R., 2023. The overlooked contribution of trees outside forests to tree cover and woody biomass across Europe. *Science Advances* 9, eadh4097. URL: <https://www.science.org/doi/10.1126/sciadv.adh4097>, doi:10.1126/sciadv.adh4097. publisher: American Association for the Advancement of Science.
- Lukeš, P., Myroniuk, V., Shamrai, A., Melnichenko, V., Schwartz, M., Pauls, J., 2025. Integrating Global Canopy Height Models with Satellite Data for Improved Forest Inventory in Ukraine. URL: <https://papers.ssrn.com/abstract=5495040>, doi:10.2139/ssrn.5495040.
- Mermoz, S., Prieto, J.D., Planells, M., Morin, D., Koleck, T., Mouret, F., Bouvet, A., Le Toan, T., Sheeren, D., Hamrouni, Y., Bélouard, T., Paillassa, É., Carme, M., Chartier, M., Martel, S., Féret, J.B., 2024. Submonthly Assessment of Temperate Forest Clear-Cuts in Mainland France. *IEEE Journal of Selected Topics in Applied Earth Observations and Remote Sensing* 17, 13743–13764. URL: <https://ieeexplore.ieee.org/abstract/document/10604724>, doi:10.1109/JSTARS.2024.3429012. conference Name: IEEE Journal of Selected Topics in Applied Earth Observations and Remote Sensing.
- Moffette, F., Alix-Garcia, J., Shea, K., Pickens, A.H., 2021. The impact of near-real-time deforestation alerts across the tropics. *Nature Climate Change* 11, 172–178. URL: <https://www.nature.com/art>

- icles/s41558-020-00956-w, doi:10.1038/s41558-020-00956-w. publisher: Nature Publishing Group.
- Moreau, G., Chagnon, C., Achim, A., Caspersen, J., D'Orangeville, L., Sánchez-Pinillos, M., Thiffault, N., 2022. Opportunities and limitations of thinning to increase resistance and resilience of trees and forests to global change. *Forestry: An International Journal of Forest Research*, cpac010URL: <https://academic.oup.com/forestry/advance-article/doi/10.1093/forestry/cpac010/6561434>, doi:10.1093/forestry/cpac010.
- Mosig, C., 2026. Mapping sub-pixel forest disturbances from Sentinel-2 timeseries.
- Mosig, C., Vajna-Jehle, J., Mahecha, M.D., Cheng, Y., Hartmann, H., Montero, D., Junttila, S., Horion, S., Schwenke, M.B., Koontz, M.J., Maulud, K.N.A., Adu-Bredu, S., Al-Halbouni, D., Ali, M., Allen, M., Altman, J., Amorós, L., Angiolini, C., Astrup, R., Awada, H., Barrasso, C., Bartholomeus, H., Beck, P.S., Bozzini, A., Braun-Wimmer, J., Brede, B., Breunig, F.M., Brugnaro, S., Buras, A., Burchard-Levine, V., Camarero, J.J., Candotti, A., Capuder, L., Carrieri, E., Centritto, M., Chirici, G., Cloutier, M., Conciani, D., Cushman, K., Dalling, J.W., Dao, P.D., Dempewolf, J., Denter, M., Dogotari, M., Díaz-Delgado, R., Ecke, S., Eichel, J., Eltner, A., Fabbri, A., Fabi, M., Fassnacht, F., Ferreira, M.P., Fischer, F.J., Frey, J., Frick, A., Fuentes, J., Ganz, S., Garbarino, M., García, M., Gassiloud, M., Gazol, A., Gea-Izquierdo, G., Gerberding, K., Ghasemi, M., Giannetti, F., Gillan, J., Gonzalez, R., Gosper, C., Greene, T., Greinwald, K., Grieve, S., Große-Stoltenberg, A., Gutierrez, J.A., Göritz, A., Hajek, P., Hedding, D., Hempel, J., Heremans, S., Hernández, M., Heurich, M., Honkavaara, E., Höfle, B., Jackisch, R., Jucker, T., Kalwij, J.M., Kepfer-Rojas, S., Khatri-Chhetri, P., Kleinebecker, T., Klemmt, H.J., Klouček, T., Koivumäki, N., Kolagani, N., Komárek, J., Korznikov, K., Kraszewski, B., Kruse, S., Krüger, R., Kuechly, H., Kwong, I.H., Laliberté, E., Langan, L., Latifi, H., Leal-Medina, C., Lehmann, J.R., Li, L., Lines, E., Lisiewicz, M., Lopatin, J., Lucieer, A., Ludwig, A., Ludwig, M., Lyytikäinen-Saarenmaa, P., Ma, Q., Mansuy, N., Peña, J.M., Marino, G., Maroschek, M., Martín, M., Martín-Benito, D., Matham, P., Mazzoni, S., Meloni, F., Menzel, A., Meyer, H., Miraki, M., Moreno, G., Moreno-Fernández, D., Muller-Landau, H.C., Mälicke, M., Möhring, J., Müllerova, J., Naidu, S.S., Nardi, D., Neumeier, P., Nita, M.D., Näsi, R., Oppgenoorth, L., Orunbaev, S., Palmer, M., Paul, T., Pfenning, M., Potts, A., Prasanna, G.L., Prober, S., Puliti, S., Pérez-Luque, A.J., Pérez-Priego, O., Reudenbach, C., Revuelto, J., Rivas-Torres, G., Roberge, P., Roggero, P.P., Rossi, C., Ruehr, N.K., Ruiz-Benito, P., Runge, C.M., Satta, G.G.A., Scanu, B., Scherer-Lorenzen, M., Schiefer, F., Schiller, C., Schladebach, J., Schmehl, M.T., Schmid, J., Schmidt, T.A., Schwarz, S., Seidl, R., Seifert, T., Barba, A.S., Shafeian, E., Shapiro, A., De Simone, L., Sohrobi, H., Soltani, S., Sotomayor, L., Sparrow, B., Steer, B.S., Stenson, M., Stöckigt, B., Su, Y., Suomalainen, J., Tamudo, E., Barbieri, M.J.T., Tomelleri, E., Torresani, M., Trepikli, K., Ullah, S., Ullah, S., Umlauf, J., Vargas-Ramírez, N., Vatandaslar, C., Visacki, V., Volpi, M., Vásquez, V., Wallis, C., Weinstein, B., Weiser, H., Wich, S., Ximena, T.C., Zarco-Tejada, P.J., Zdunic, K., Zielewska-Büttner, K., De Oliveira, R.A., Van Wagendonk, L., Von Dosky, V., Kattenborn, T., 2026. deadtrees.earth — An open-access and interactive database for centimeter-scale aerial imagery to uncover global tree mortality dynamics. *Remote Sensing of Environment* 332, 115027. URL: <https://linkinghub.elsevier.com/retrieve/pii/S0034425725004316>, doi:10.1016/j.rse.2025.115027.
- Mullissa, A., Saatchi, S., Dalagnol, R., Erickson, T., Provost, N., Osborn, F., Ashary, A., Moon, V., Melling, D., 2024. LUCA: A Sentinel-1 SAR-Based Global Forest Land Use Change Alert. *Remote Sensing* 16, 2151. URL: <https://www.mdpi.com/2072-4292/16/12/2151>, doi:10.3390/rs16122151. publisher: Multidisciplinary Digital Publishing Institute.
- Myroniuk, V., Weinreich, A., Von Dosky, V., Melnychenko, V., Shamrai, A., Matsala, M., Gregory, M.J., Bell, D.M., Davis, R., 2024. Nationwide remote sensing framework for forest resource assessment in war-affected Ukraine. *Forest Ecology and Management* 569, 122156. URL: <https://linkinghub.elsevier.com/retrieve/pii/S0378112724004687>, doi:10.1016/j.foreco.2024.122156.
- Network, I.T.M., 2025. Towards a global understanding of tree mortality. *New Phytologist* 245, 2377–2392. URL: <https://onlinelibrary.wiley.com/doi/abs/10.1111/nph.20407>, doi:10.1111/nph.20407. eprint: <https://nph.onlinelibrary.wiley.com/doi/pdf/10.1111/nph.20407>.

- Nilsson, M., Nordkvist, K., Jonzén, J., Lindgren, N., Axensten, P., Wallerman, J., Egberth, M., Larsson, S., Nilsson, L.L., Eriksson, J., Olsson, H., Olsson, H., 2017. A nationwide forest attribute map of Sweden predicted using airborne laser scanning data and field data from the National Forest Inventory. *Remote Sensing of Environment* 194, 447–454. doi:10.1016/j.rse.2016.10.022. mAG ID: 2537499819.
- Nolet, P., Kneeshaw, D., Messier, C., Béland, M., 2018. Comparing the effects of even- and uneven-aged silviculture on ecological diversity and processes: A review. *Ecology and Evolution* 8, 1217–1226. URL: <https://onlinelibrary.wiley.com/doi/abs/10.1002/ece3.3737>, doi:10.1002/ece3.3737. eprint: <https://onlinelibrary.wiley.com/doi/pdf/10.1002/ece3.3737>.
- Ols, C., Hervé, J.C., Bontemps, J.D., 2020. Recent growth trends of conifers across Western Europe are controlled by thermal and water constraints and favored by forest heterogeneity. *Science of The Total Environment* 742, 140453. URL: <https://linkinghub.elsevier.com/retrieve/pii/S0048969720339759>, doi:10.1016/j.scitotenv.2020.140453.
- Pan, Y., Birdsey, R.A., Phillips, O.L., Houghton, R.A., Fang, J., Kauppi, P.E., Keith, H., Kurz, W.A., Ito, A., Lewis, S.L., Nabuurs, G.J., Shvidenko, A., Hashimoto, S., Lerink, B., Schepaschenko, D., Castanho, A., Murdiyarsa, D., 2024. The enduring world forest carbon sink. *Nature* 631, 563–569. URL: <https://www.nature.com/articles/s41586-024-07602-x>, doi:10.1038/s41586-024-07602-x. publisher: Nature Publishing Group.
- Pauls, J., Zimmer, M., Turan, B., Saatchi, S., Ciais, P., Pokutta, S., Gieseke, F., 2025. Capturing Temporal Dynamics in Large-Scale Canopy Tree Height Estimation. URL: <https://openreview.net/forum?id=ri1cs3vtXX>.
- Pontes-Lopes, A., Dalagnol, R., Dutra, A.C., de Jesus Silva, C.V., de Alencastro Graça, P.M.L., de Oliveira e Cruz de Aragão, L.E., 2022. Quantifying Post-Fire Changes in the Aboveground Biomass of an Amazonian Forest Based on Field and Remote Sensing Data. *Remote Sensing* 14, 1545. URL: <https://www.mdpi.com/2072-4292/14/7/1545>, doi:10.3390/rs14071545. publisher: Multidisciplinary Digital Publishing Institute.
- Rahimizadeh, N., Babaie Kafaky, S., Sahebi, M.R., Mataji, A., 2019. Forest structure parameter extraction using SPOT-7 satellite data by object- and pixel-based classification methods. *Environmental Monitoring and Assessment* 192, 43. URL: <https://doi.org/10.1007/s10661-019-8015-x>, doi:10.1007/s10661-019-8015-x.
- Ramirez Parra, L.A., Renaud, J.P., Vega, C., 2024. How reliable are remote sensing maps calibrated over large areas? A matter of scale? URL: <http://arxiv.org/abs/2408.03953>, doi:10.48550/arXiv.2408.03953. arXiv:2408.03953 [stat].
- Reiche, J., Mullissa, A., Slagter, B., Gou, Y., Tsendbazar, N.E., Odongo-Braun, C., Vollrath, A., Weisse, M.J., Stolle, F., Pickens, A., Donchyts, G., Clinton, N., Gorelick, N., Herold, M., 2021. Forest disturbance alerts for the Congo Basin using Sentinel-1. *Environmental Research Letters* 16, 024005. URL: <https://dx.doi.org/10.1088/1748-9326/abd0a8>, doi:10.1088/1748-9326/abd0a8. publisher: IOP Publishing.
- Risbøl, O., Langhammer, D., Schlosser Mauritsen, E., Seitsonen, O., 2020. Employment, Utilization, and Development of Airborne Laser Scanning in Fennoscandinavian Archaeology—A Review. *Remote Sensing* 12, 1411. URL: <https://www.mdpi.com/2072-4292/12/9/1411>, doi:10.3390/rs12091411. publisher: Multidisciplinary Digital Publishing Institute.
- Ritter, F., Ciais, P., Senf, C., Santoro, M., Xu, Y., Pelissier-Tanon, A., Schwartz, M., Fayad, I., Carvalho, N., Brandt, M., Fensholt, R., Besnard, S., Avitabile, V., 2025. Alarming decline in the carbon sink of European forests driven by disturbances. URL: <https://www.researchsquare.com/article/rs-3671432/v1>, doi:10.21203/rs.3.rs-3671432/v1. iISSN: 2693-5015.
- Saarela, S., Wästlund, A., André Wästlund, Holmström, E., Mensah, A.A., Holm, S., Nilsson, M., Fridman, J., Ståhl, G., 2020. Mapping aboveground biomass and its prediction uncertainty using LiDAR and field data, accounting for tree-level allometric and LiDAR model errors. *Forest Ecosystems* 7, 1–17. doi:10.1186/s40663-020-00245-0. mAG ID: 3039816702.
- Schwartz, M., Ciais, P., De Truchis, A., Chave, J., Otlé, C., Vega, C., JP., W., Nicolas, M., Jouaber, S., Liu, S., Saatchi, S., Brandt, M., Fayad, I., 2023. FORMS: Forest Multiple Source height, wood volume, and

- biomass maps in France at 10 to 30 m resolution based on Sentinel-1, Sentinel-2, and GEDI data with a deep learning approach. URL: <https://zenodo.org/record/7840108>, doi:10.5281/ZENODO.7840108.
- Schwartz, M., Ciais, P., Sean, E., De Truchis, A., Vega, C., Besic, N., Fayad, I., Wigneron, J.P., Brood, S., Pelissier-Tanon, A., Pauls, J., Belouze, G., Xu, Y., 2025. Retrieving yearly forest growth from satellite data: A deep learning based approach. *Remote Sensing of Environment* 330, 114959. URL: <https://linkinghub.elsevier.com/retrieve/pii/S0034425725003633>, doi:10.1016/j.rse.2025.114959.
- Senf, C., Pflugmacher, D., Zhiqiang, Y., Sebal, J., Knorn, J., Neumann, M., Hostert, P., Seidl, R., 2018. Canopy mortality has doubled in Europe's temperate forests over the last three decades. *Nature Communications* 9, 4978. URL: <https://www.nature.com/articles/s41467-018-07539-6>, doi:10.1038/s41467-018-07539-6. number: 1 Publisher: Nature Publishing Group.
- Serra, J.P., 1982. *Image Analysis and Mathematical Morphology*. Academic Press. Google-Books-ID: BpdTAAAYAAJ.
- Shi, Y., Wang, J., Kissling, W.D., 2025. Multi-temporal high-resolution data products of ecosystem structure derived from country-wide airborne laser scanning surveys of the Netherlands. *Earth System Science Data* 17, 3641–3677. URL: <https://essd.copernicus.org/articles/17/3641/2025/>, doi:10.5194/essd-17-3641-2025. publisher: Copernicus GmbH.
- Shvidenko, A., Nilsson, S., 2002. Dynamics of Russian Forests and the Carbon Budget in 1961–1998: An Assessment Based on Long-Term Forest Inventory Data. *Climatic Change* 55, 5–37. URL: <https://doi.org/10.1023/A:1020243304744>, doi:10.1023/A:1020243304744.
- Su, Y., Schwartz, M., Fayad, I., García, M., Zavala, M.A., Tijerín-Triviño, J., Astigarraga, J., Cruz-Alonso, V., Liu, S., Zhang, X., Chen, S., Ritter, F., Besic, N., d'Aspremont, A., Ciais, P., 2025. Canopy height and biomass distribution across the forests of Iberian Peninsula. *Scientific Data* 12, 678. URL: <https://www.nature.com/articles/s41597-025-05021-9>, doi:10.1038/s41597-025-05021-9. publisher: Nature Publishing Group.
- Tolan, J., Yang, H.I., Nosarzewski, B., Couairon, G., Vo, H., Brandt, J., Spore, J., Majumdar, S., Haziza, D., Vamaraju, J., Moutakanni, T., Bojanowski, P., Johns, T., White, B., Tieceke, T., Couprie, C., 2023. Sub-meter resolution canopy height maps using self-supervised learning and a vision transformer trained on Aerial and GEDI Lidar. URL: <http://arxiv.org/abs/2304.07213>, doi:10.48550/arXiv.2304.07213. arXiv:2304.07213 [cs].
- Tomppo, E., Haakana, M., Katila, M., Peräsaari, J., 2008. *Multi-Source National Forest Inventory: Methods and Applications*. Springer Science & Business Media. Google-Books-ID: hvyPkFi0GBQC.
- Tucker, C., Brandt, M., Hiernaux, P., Kariryaa, A., Rasmussen, K., Small, J., Igel, C., Reiner, F., Melocik, K., Meyer, J., Sinno, S., Romero, E., Glennie, E., Fitts, Y., Morin, A., Pinzon, J., McClain, D., Morin, P., Porter, C., Loeffler, S., Kergoat, L., Issoufou, B.A., Savadogo, P., Wigneron, J.P., Poulter, B., Ciais, P., Kaufmann, R., Myneni, R., Saatchi, S., Fensholt, R., 2023. Sub-continental-scale carbon stocks of individual trees in African drylands. *Nature* 615, 80–86. URL: <https://www.nature.com/articles/s41586-022-05653-6>, doi:10.1038/s41586-022-05653-6. number: 7950 Publisher: Nature Publishing Group.
- Turubanova, S., Potapov, P., Hansen, M.C., Li, X., Tyukavina, A., Pickens, A.H., Hernandez-Serna, A., Arranz, A.P., Guerra-Hernandez, J., Senf, C., Häme, T., Valbuena, R., Eklundh, L., Brovkina, O., Navrátilová, B., Novotný, J., Harris, N., Stolle, F., 2023. Tree canopy extent and height change in Europe, 2001–2021, quantified using Landsat data archive. *Remote Sensing of Environment* 298, 113797. URL: <https://www.sciencedirect.com/science/article/pii/S0034425723003486>, doi:10.1016/j.rse.2023.113797.
- Vallet, L., Schwartz, M., Ciais, P., van Wees, D., de Truchis, A., Mouillot, F., 2023. High resolution data reveal a surge of biomass loss from temperate and Atlantic pine forests, seizing the 2022 fire season distinctiveness in France. *EGUsphere*, 1–39 URL: <https://egusphere.copernicus.org/preprints/2023/egusphere-2023-529/>, doi:10.5194/egusphere-2023-529. publisher: Copernicus GmbH.
- Vehmas, M., Packalén, P., Maltamo, M., Eerikäinen, K., 2011. Using airborne laser scanning data for detecting canopy gaps and their understory type in mature

- boreal forest. *Annals of Forest Science* 68, 825–835. URL: <https://doi.org/10.1007/s13595-011-0079-x>, doi:10.1007/s13595-011-0079-x.
- Vepakomma, U., St-Onge, B., Kneeshaw, D., 2008. Spatially explicit characterization of boreal forest gap dynamics using multi-temporal lidar data. *Remote Sensing of Environment* 112, 2326–2340. URL: <https://linkinghub.elsevier.com/retrieve/pii/S0034425707004531>, doi:10.1016/j.rse.2007.10.001.
- Viana-Soto, A., Senf, C., 2025. The European Forest Disturbance Atlas: a forest disturbance monitoring system using the Landsat archive. *Earth System Science Data* 17, 2373–2404. URL: <https://essd.copernicus.org/articles/17/2373/2025/>, doi:10.5194/essd-17-2373-2025. publisher: Copernicus GmbH.
- Wang, W., Xie, E., Li, X., Fan, D.P., Song, K., Liang, D., Lu, T., Luo, P., Shao, L., 2022. PVT v2: Improved baselines with Pyramid Vision Transformer. *Computational Visual Media* 8, 415–424. URL: <https://doi.org/10.1007/s41095-022-0274-8>, doi:10.1007/s41095-022-0274-8.
- White, J.C., Tompalski, P., Coops, N.C., Wulder, M.A., 2018. Comparison of airborne laser scanning and digital stereo imagery for characterizing forest canopy gaps in coastal temperate rainforests. *Remote Sensing of Environment* 208, 1–14. URL: <https://linkinghub.elsevier.com/retrieve/pii/S0034425718300087>, doi:10.1016/j.rse.2018.02.002.
- Ygorra, B., Frappart, F., Wigneron, J., Moisy, C., Catry, T., Baup, F., Hamunyela, E., Riazanoff, S., 2021. Monitoring loss of tropical forest cover from Sentinel-1 time-series: A CuSum-based approach. *International Journal of Applied Earth Observation and Geoinformation* 103, 102532. URL: <https://linkinghub.elsevier.com/retrieve/pii/S0303243421002397>, doi:10.1016/j.jag.2021.102532.